People`s Democratic Republic of Algeria

Ministry of Higher Education and Scientific Research

University of Echahid Hamma Lakhdar - El Oued

Faculty of Technology

Department of Process Engineering & Petrochemistry

Dissertation

ACADEMIC MASTER

Domain: Science and Technology

Division: Process Engineering

Specialty: Chemical Engineering

Presented by:

Wassim Soltani

Azedinne Kir

Entitled:

Literature analysis of the factors affecting the adsorption of heavy metals by nanomaterials

Dissertation Submitted in Partial Fulfillment of the Requirements for the Master Degree in ……...

Publicly defended in: 13/06/2026

Board of Examiners:

Dr. Ben Amara Hassan	**President**
Dr. Meneceur Souhaila	**Supervisor**
Dr. Chaima Salmi	**Co_Supervisor**
Dr. Chaabia Nacer	**Examiner**

Academic Year: 2025/2026

DEDICATION

To the one who crowned me with pride and honor

To the one who taught me that the taste of success comes only after the bitterness of struggle, and that reaching the top requires determination... To the one with the big heart and generous hand, who dedicated his life so that I could reach this moment, and who was an unwavering support in every step I took... My dear father, may God protect him, grant him a long life, and reward him abundantly

To the inexhaustible wellspring of tenderness and giving

To the one whose prayers paved the way for my success, whose sincere supplications in the dead of night overcame every obstacle I faced... To the one who stayed up nights so I could rest, and toiled so I could be happy, my paradise on earth, the secret to my success, and the balm for my wounds... My beloved mother, may God clothe her in health and well-being and keep her as a light in our lives

To those from whom I draw resolve and strength

To those who shared the pulse of life with me, and were my best companions on the path of childhood and youth... To those who stand by me in hardship as well as ease My brothers and sisters, each by name and position, may God protect and preserve you, and perpetuate the bonds of affection and love between us.

To those who illuminated my path with knowledge,

To everyone who taught me a single letter, which became a beacon illuminating my way, and planted within me an unquenchable ambition... my esteemed teachers,

To all of you... I dedicate this humble scientific effort and from the bottom of my heart,

thank you.

ACKNOWLEDGEMENTS

First and foremost, we thank God Almighty for His countless blessings and for granting us the strength and determination to complete this work.

we would like to express our sincere gratitude and appreciation to our supervisor, ***Dr. Chaima Salmi*** *and* ***Dr. Meneceur Souhaila*** *we are deeply grateful for their invaluable guidance, unwavering support, and remarkable patience throughout this research. Their thorough explanations, insightful advice, and willingness to dedicate their time and expertise were fundamental to the success of this work. It was an honor to work under their supervision, and we thank them from the bottom of our hearts for their dedication and encouragement, which motivated us to give our best.*

Finally, we extend our sincere thanks to the esteemed members of the judging panel for accepting to evaluate this work and for the time they dedicated to reviewing it. Their scholarly observations and suggestions will undoubtedly enrich the quality of this research.

we also extend our sincere thanks and gratitude to all the faculty members of the Department of Process and Petrochemical Engineering, especially those specializing in Chemical Engineering at the Faculty of Science and Technology, ***University of El Oued****, for the knowledge and solid academic foundation they provided us throughout our years of study.*

Finally, we would like to thank everyone who contributed, directly or indirectly, with kind words or a helping hand, to the completion of this research.

ABSTRACT

This thesis explores the theoretical analysis and literature review concerning the green synthesis, characterization, and environmental applications of metal oxide-based nanocomposites for the effective removal of complex pollutants from aqueous media. The work is framed within the context of sustainable nanotechnology and focuses on multifunctional nanocomposite systems combining metal oxide nanoparticles with biopolymers or magnetic structures to enhance photocatalytic and adsorptive performance.

Several innovative nanocomposite systems were comprehensively analyzed and evaluated:

1. • **MgO@SnO_2/PVP** nanocomposites for the adsorption of heavy metals, oil-in-water (OIW) emulsions, and total suspended solids (TSS) from industrial petroleum wastewater.
2. • **Ca/α-Fe_2O_3/ZnO/CuO** quaternary nanocomposites for high-efficiency heavy metal removal from contaminated sludge.
3. • **CS/Fe_3O_4** (chitosan-coated) and **Ag@Fe_3O_4** nanocomposites for the simultaneous removal of heavy metals and rapid photodegradation of organic dyes (Methylene Blue and Rose Bengal).
4. • **ZnO@CuO** heterojunctions and single metal oxides (**α-Fe_2O_3, CuO, ZnO**) for the degradation of total petroleum hydrocarbons (TPH) and advanced purification of real petroleum effluents.

All nanomaterials were synthesized using eco-friendly routes, employing natural plant extracts (*Mentha pulegium*, *Laurus nobilis*, *Pistacia lentiscus*, and *Portulaca oleracea*) as reducing and capping agents. Structural, morphological, optical, and surface properties were characterized using XRD, FTIR, SEM, EDX, UV–Vis spectroscopy, and zeta potential analysis. The performance of the nanocomposites was evaluated through adsorption and photodegradation experimental data. Kinetic (pseudo-first and pseudo-second-order) and isotherm (Langmuir and Freundlich) models were applied to describe the adsorption mechanisms.

Keywords: Green synthesis, Metal oxide nanoparticles, Petroleum wastewater, Heavy metals adsorption, Photocatalytic degradation, Sustainable nanotechnology.

الملخص

تتناول هذه المذكرة (مراجعة أدبية وتحليل نظري) موضوع التخليق الأخضر، والتوصيف، والتطبيقات البيئية للمواد النانوية المركبة لأكاسيد المعادن، بهدف إزالة الملوثات المعقدة بكفاءة من الأوساط المائية .يندرج هذا العمل ضمن إطار تكنولوجيا النانو المستدامة، ويركز على تقييم أنظمة نانوية متعددة الوظائف تجمع بين جسيمات أكاسيد المعادن وبوليمرات حيوية أو هياكل مغناطيسية لتحسين الأداء التحفيزي الضوئي والامتزازي.

تم تحليل وتقييم عدة أنظمة نانوية مركبة مبتكرة بشكل دراسة معمقة :

1- مركب **(MgO@SnO2/PVP)** لامتزاز المعادن الثقيلة، الزيوت، والمواد العالقة من مياه الصرف الصناعي البترولي .
2- المركب الرباعي **(Ca/α-Fe2O3/ZnO/CuO)** لإزالة المعادن الثقيلة بكفاءة عالية جداً من الحمأة الملوثة .
3- مركبات **(Ag@Fe3O4)** و **(CS/Fe3O4 المغلفة بالشيتوزان)** للإزالة المتزامنة للمعادن الثقيلة والتحلل الضوئي السريع للأصباغ العضوية (أزرق الميثيلين، وردي البنغال) .
4- الوصلة غير المتجانسة **(ZnO@CuO)** والجسيمات الأحادية **(α-Fe2O3, CuO, ZnO)** لتفكيك الهيدروكربونات والتنقية المتقدمة للمياه البترولية الحقيقية.

تم تخليق جميع هذه المواد باستخدام طرق صديقة للبيئة، معتمدة على مستخلصات نباتية (مثل النعناع، الغار، الضرو، والبقلة) كعوامل اختزال وتغليف .تم توصيف الخصائص البنيوية والمورفولوجية والبصرية والسطحية باستخدام تقنياتXRD ، FTIR، SEM، EDX، UV-Vis، وقياس الجهد السطحي (Zeta potential) .كما تم تقييم الأداء من خلال تجارب الامتزاز والتحلل الضوئي، مع تطبيق نماذج حركية (الرتبة الأولى والثانية الكاذبة) ونماذج توازن الامتزاز (لانغمويير وفروندليش) لفهم آليات التفاعل.

أظهرت النتائج التحليلية فعالية استثنائية تصل إلى 100% في إزالة المعادن الثقيلة والملوثات، مع سهولة الفصل المغناطيسي، وثباتًا هيكليًا ممتازًا على مدى عدة دورات متتالية لإعادة الاستخدام .يقدم هذا البحث النظري رؤى علمية قيمة لتصميم مواد نانوية خضراء تُستخدم في المعالجة المتقدمة لمياه الصرف الصناعية، مما يسهم في تقدم تكنولوجيا النانو المستدامة وحماية البيئة .

الكلمات المفتاحية: التخليق الأخضر، جسيمات أكاسيد المعادن النانوية، مياه الصرف البترولية، امتصاص المعادن الثقيلة، التحلل التحفيزي الضوئي، المركبات النانوية.

TABLE OF CONTENTS

Chapter III. Results and Performance Evaluation of the Synthesized Nanomaterials

LIST OF FIGURES

Chapter I. Introduction to Green Nanotechnology for Environmental Remediation

Chapter II. Experimental Methods for Nanocomposite Synthesis and Characterization

Chapter III. Results and Performance Evaluation of the Synthesized Nanomaterials

LIST OF TABLES

Chapter I. Introduction to Green Nanotechnology for Environmental Remediation

Chapter II. Experimental Methods for Nanocomposite Synthesis and Characterization

Chapter III. Performance Analysis and Characterization of the Reviewed Nanomaterials

LIST OF ABBREVIATIONS

A^0: Initial optical absorbance value (UV-Vis spectrophotometric analysis).

Ag: Silver.

$AgNO_3$: Silver nitrate.

As: Arsenic.

As^{3+}: Trivalent arsenic ion.

As^{5+}: Pentavalent arsenic ion.

At: Optical absorbance at time t (UV-Vis spectrophotometric analysis).

Be: Beryllium.

Be^{2+}: Divalent beryllium ion.

Bi: Bismuth.

Bi^{2+}: Divalent bismuth ion.

BOD: Biochemical Oxygen Demand.

BTEX: Benzene, Toluene, Ethylbenzene, and Xylenes.

C=O: Carbonyl functional group (FTIR absorption 1700–1750 cm^{-1}).

C_0: Initial concentration of pollutant (mg/L).

Ca: Calcium.

Cd: Cadmium.

Cd^{2+}: Divalent cadmium ion.

Ce: Equilibrium concentration of pollutant in solution (mg/L).

cm^{-1}: Reciprocal centimeters (wavenumber unit in FTIR spectroscopy).

COD: Chemical Oxygen Demand.

Cr: Chromium.

Cr^{3+}: Trivalent chromium ion.

Cr^{6+}: Hexavalent chromium ion.

CS: Chitosan.

Ct: Concentration of pollutant at time t (mg/L).

Cu: Copper.

Cu Kα: Copper K-alpha X-ray radiation (λ = 1.5406 Å); source used in XRD analysis.

Cu^{2+}: Divalent copper ion.

CuO: Copper (II) oxide.

D%: Photocatalytic degradation efficiency (percentage).

DNA: Deoxyribonucleic acid.

DO: Dissolved Oxygen.

EDS: Energy Dispersive Spectroscopy.

EDX: Energy Dispersive X-ray Spectroscopy.

Eg: Optical energy band gap (eV); determined via Tauc plot from UV-Vis data.

eV: Electron Volt.

Fe: Iron.

Fe_2O_3: Iron (III) oxide (hematite).

Fe_3O_4: Iron (II,III) oxide (magnetite).

Fe^{3+}: Trivalent iron ion.

FTIR: Fourier-Transform Infrared Spectroscopy.

g: Gram.

GAE: Gallic Acid Equivalent (unit for total phenolic content, mg GAE/g).

h: Hour.

H^+: Proton (hydrogen ion); used in pH adjustment and desorption processes.

HCl: Hydrochloric acid.

HNO_3: Nitric acid.

k2: Rate constant of pseudo-second-order adsorption (g/mg·min).

KBr: Potassium bromide (used for FTIR pellet preparation).

Kf: Freundlich adsorption capacity constant.

KL: Langmuir adsorption equilibrium constant (L/mg).

kV: Kilovolt.

L: Liter.

m: Meter; also: mass of adsorbent used in batch experiment (g).

M-O: Metal-Oxygen bond stretching vibration (FTIR, 400–800 cm^{-1}).

MB: Methylene Blue (organic dye).

Mg: Magnesium.

Mg^{2+}: Divalent magnesium ion.

mg: Milligram.

mg/g: Milligrams per gram (unit of adsorption capacity).

mg/L: Milligrams per liter (unit of pollutant concentration).

MgO: Magnesium oxide.

mL: Milliliter.

Mn: Manganese.

Mn^{2+}: Divalent manganese ion.

Mo: Molybdenum.

Mo^{2+}: Molybdenum ion.

mV: Millivolt.

NaOH: Sodium hydroxide.

NCs: Nanocomposites.

NH_2: Amine functional group ($–NH_2$); present in chitosan structure.

Ni: Nickel.

Ni^{2+}: Divalent nickel ion.

nm: Nanometer.

NPs: Nanoparticles.

O-H: Hydroxyl functional group (O-H stretching vibration, FTIR 3200–3600 cm^{-1}).

O_2^-: Superoxide anion radical (reactive oxygen species in photocatalysis).

OH: Hydroxyl radical (reactive oxygen species generated during photocatalysis).

OIW: Oil-in-Water (emulsion).

PAHs: Polycyclic Aromatic Hydrocarbons.

Pb: Lead.

Pb^{2+}: Divalent lead ion.

pH: Potential of Hydrogen (measure of acidity/alkalinity of a solution).

POPs: Persistent Organic Pollutants.

PVDF: Polyvinylidene fluoride (ultrafiltration membrane material).

PVP: Polyvinylpyrrolidone.

qe: Equilibrium adsorption capacity (mg/g).

qm: Maximum monolayer adsorption capacity — Langmuir model (mg/g).

qt: Adsorption capacity at time t (mg/g).

R%: Pollutant removal efficiency (percentage).

RB: Rhodamine B (organic dye).

ROS: Reactive Oxygen Species.

rpm: Revolutions per minute.

Sb: Antimony.

Sb^{3+}: Trivalent antimony ion.

Se: Selenium.

Se^{2-}: Selenide ion.

SEM: Scanning Electron Microscopy.

SH: Sulfhydryl group (–SH); binding site for heavy metal toxicity in enzymes.

Sn: Tin.

Sn^{2+}: Divalent tin ion.

SnO_2: Tin (IV) oxide.

t: Contact time / reaction time (minutes or hours).

$t_{1/2}$: Half-life (time required for 50% degradation of a pollutant).

TB: Toluidine Blue (organic dye).

TiO_2: Titanium dioxide (general photocatalytic model semiconductor).

TPH: Total Petroleum Hydrocarbons.

TSS: Total Suspended Solids.

UV-Vis : Ultraviolet-Visible Spectroscopy.

V: Volt; also: Volume of solution used in adsorption experiment (L).

W: Watt.

XRD: X-Ray Diffraction.

Zn : Zinc.

Zn^{2+} : Divalent zinc ion.

ZnO: Zinc oxide.

1/ne: Freundlich adsorption intensity constant (surface heterogeneity indicator).

2θ: Two-theta (Bragg diffraction angle in XRD analysis, degrees).

°C: Degrees Celsius.

Å: Angstrom (1 Å = 10^{-10} m); used for XRD wavelength and crystallite spacing.

α-Fe_2O_3: Alpha-hematite (alpha phase of iron (III) oxide).

ΔG°: Standard Gibbs free energy change (thermodynamic parameter).

ΔH°: Standard enthalpy change (thermodynamic parameter).

ΔS°: Standard entropy change (thermodynamic parameter).

θ: Theta — Bragg diffraction angle (degrees) in XRD analysis.

λ: Wavelength (nm); for Cu Kα radiation, λ = 1.5406 Å.

General Introduction

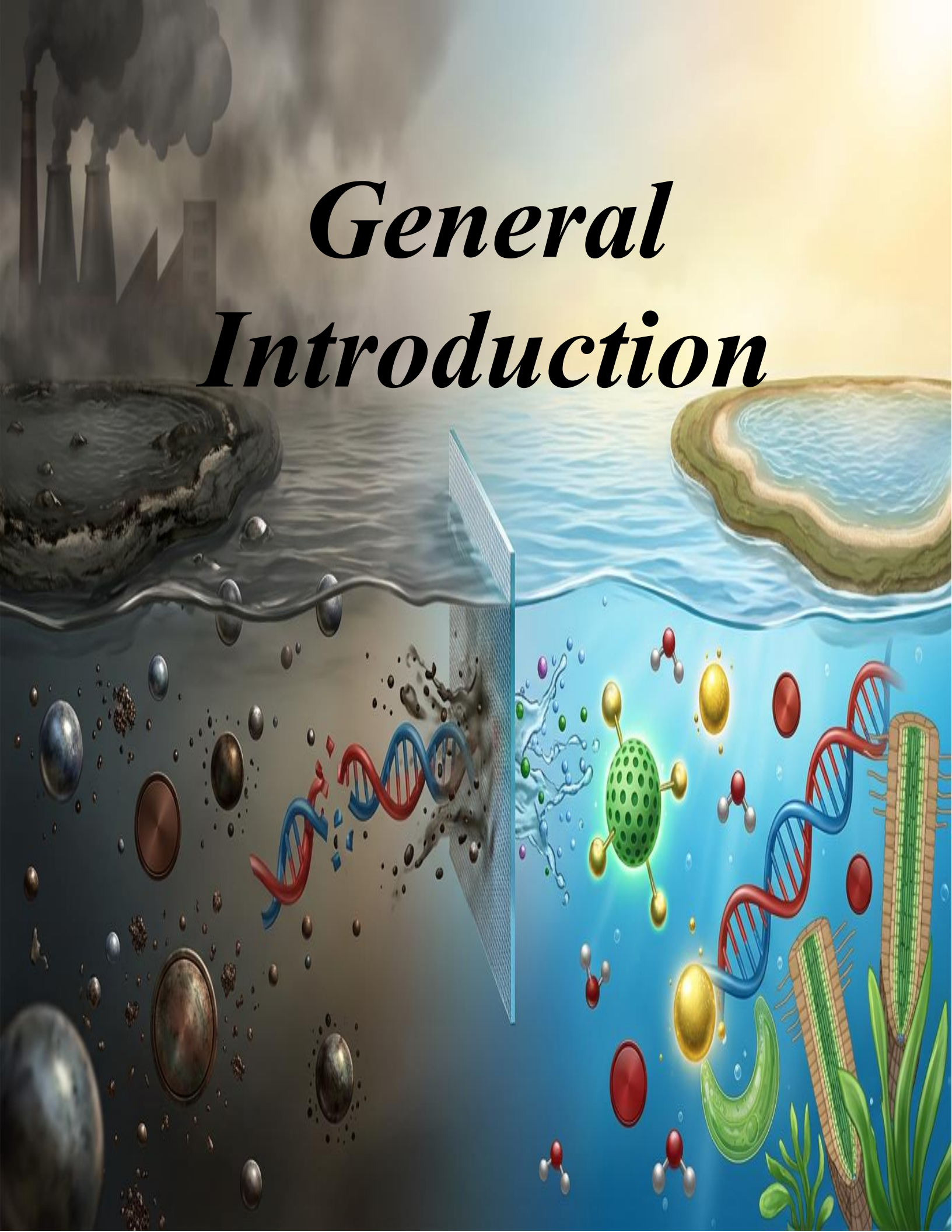

General Introduction

The continuous push for unprecedented industrial development, alongside a rapidly growing global population, has placed immense and unsustainable pressure on our finite freshwater resources[1]. Aligning with the United Nations Sustainable Development Goals, particularly the mandate for clean water and sanitation, addressing this crisis has become a paramount global priority. Every year, billions of tons of untreated industrial and petroleum effluents are discharged into global aquatic ecosystems. We are not just dealing with simple pollution; this waste is a highly complex matrix of extremely toxic heavy metals (like Pb^{2+}, Cd^{2+}, Cr^{6+}, Ni^{2+}, and As^{3+}), persistent organic dyes, stable suspended oils, and tough-to-break-down polycyclic aromatic hydrocarbons [2,3,4,5]. What makes these contaminants particularly dangerous is their severe environmental persistence and bioaccumulation potential[6]. They do not easily degrade, meaning they accumulate over time within the food chain, creating serious, long-lasting carcinogenic and mutagenic risks for both ecological networks and human health [3,5]. Finding a reliable, eco-friendly, and highly efficient way to remediate this contaminated water is no longer just an option, but an absolute existential necessity[7].

When evaluating the different types of industrial waste, petroleum wastewater stands out as one of the most formidable to treat. It is a stubborn, multiphase colloidal emulsion made up of dissolved organics, total petroleum hydrocarbons (TPH), and dangerously high levels of heavy metals [4,8,5]. For decades, the industry has relied heavily on standard macroscopic treatments like sand filtration, chemical coagulation, and basic biological bioreactors[9]. The harsh reality, however, is that these traditional methods profoundly struggle to handle such a diverse and chemically stable array of pollutants[10]. They are often too expensive to maintain at an industrial scale, fail to completely mineralize complex organic molecules, and consistently leave behind a highly toxic secondary chemical sludge that creates an entirely new and costly disposal problem [8,5].

This critical technological bottleneck is exactly where nanotechnology steps in to offer a revolutionary and practical solution. By engineering and shrinking materials down to the nanoscale, we unlock entirely new quantum and surface phenomena to tackle environmental pollution[11]. Metal oxide nanoparticles, specifically ZnO, α-Fe_2O_3, CuO, MgO, and SnO_2, have proven to be incredibly effective for advanced water remediation [2,8,5]. When a material is

reduced to this ultrafine size, its available surface-area-to-volume ratio increases exponentially, providing an abundance of unsaturated active sites for rapid chemical reactions [4,5].

As a result, these nanomaterials can rapidly sequester heavy metals through powerful surface electrostatic adsorption, while simultaneously utilizing their inherent photocatalytic properties to generate reactive oxygen species that break apart organic pollutants, even under normal visible light irradiation [2,3,5].

However, the traditional chemical manufacturing of these nanomaterials often relies on harsh, expensive, and toxic chemical reducing agents, which fundamentally contradicts the actual ultimate goal of environmental protection[12]. This paradox is exactly why green synthesis has emerged as such a crucial and disruptive alternative. By utilizing simple, natural plant extracts instead of toxic chemical reagents, researchers can produce these nanoparticles in a completely sustainable and biologically safe manner [13,3]. Endemic Mediterranean plants like Mentha pulegium, Portulaca oleracea, and Laurus nobilis naturally contain a rich profile of bioactive compounds, such as phenols, flavonoids, and natural biopolymers [3,8,5]. During the biogenic synthesis process, these natural phytochemicals perform a critical double duty: they instantly reduce the metal precursor ions to form the solid crystalline nanoparticles, and then they strategically wrap around them as steric capping agents[14]. This biological capping keeps the highly reactive particles stable, prevents them from agglomerating, and functionalizes their surface for better pollutant capture [2, 4, 5].

Taking this innovative concept a step further, recent research realized that combining different green materials creates an even more powerful remediation tool. While previous literature has extensively discussed the green synthesis of isolated, single-metal oxide nanoparticles, there remains a critical research gap regarding the comprehensive comparative analysis of advanced multimetallic systems. While a single metal oxide works reasonably well, engineering complex nanocomposites by mixing multiple metal oxides or integrating specific natural polymers boosts the overall performance dramatically[15]. When diverse semiconducting materials like ZnO and CuO are combined to form heterojunctions, or when a magnetic iron oxide core is coated with a biopolymer like chitosan (CS/Fe_3O_4), a profound synergistic effect occurs [13, 3, 8]. The resulting advanced composite can tackle multiple distinct contaminants simultaneously. It can aggressively pull heavy metal cations out of the water using strong electrostatic forces while actively and catalytically breaking down stubborn oil hydrocarbons and persistent organic dyes [3], [4,8,5]. An

added major practical advantage of including a superparamagnetic core is that once the wastewater is completely purified, a simple external magnetic field can instantly pull the nanomaterials out of the suspension for cyclic reuse, making the entire continuous treatment process highly economically viable [3,4].

With these significant technological advancements in mind, the primary objective of this review thesis is to provide a comprehensive, critical, and up-to-date analysis of how green-synthesized metal oxide nanocomposites are practically applied in advanced wastewater treatment. This work uniquely bridges the literature gap by critically evaluating the synergistic effects specifically optical band-gap narrowing and enhanced adsorption kinetics within engineered binary, ternary, and quaternary heterojunctions compared to conventional methods. It systematically breaks down the specific green methodologies used to synthesize these biogenic materials from natural plant precursors and meticulously examines the advanced analytical techniques required to characterize their unique structural and optical properties. Ultimately, it aims to quantify exactly how well these engineered nanomaterials perform when put to the ultimate test against real-world multiphase pollutants, specifically focusing on their demonstrated maximum capacity to rapidly eliminate heavy metals, complex petroleum hydrocarbons, and toxic dyes from highly contaminated industrial effluents.

The structure of this thesis is logically organized into the following successive sections:

- **General Introduction:** Provides the foundational global background, highlighting the critical challenges of complex petroleum wastewater, the extreme toxicity of heavy metals and organic dyes, and the significant paradigm-shifting role of plant-mediated green nanotechnology in sustainable environmental remediation.
- **Chapter I (Literature Review):** Discusses the fundamental theoretical framework, detailing the intricate composition of industrial effluents, the unique physicochemical properties of metal oxide nanoparticles at the nanoscale, and the powerful synergistic effects of biogenic multimetallic and magnetic nanocomposites.
- **Chapter II (Materials and Methods):** Details the experimental procedures and physical reagents, including the preparation of diverse aqueous plant extracts (such as Mentha pulegium and Laurus nobilis), the specific green synthesis protocols and operating parameters for the nanomaterials, and the advanced characterization instrumentation employed.

- **Chapter III (Results and Discussion):** Critically evaluates the structural, morphological, and optical properties of the synthesized nanomaterials, and comprehensively analyzes their practical performance in total pollutant removal, heavily supported by rigorous adsorption isotherms, kinetic modeling, and cyclic reusability data.
- **General Conclusion:** Summarizes the major empirical findings of the comprehensive research and outlines the most promising future perspectives and remaining engineering challenges for the large-scale continuous industrial application of these green catalysts.

Chapter I. Introduction to Green Nanotechnology for Environmental Remediation

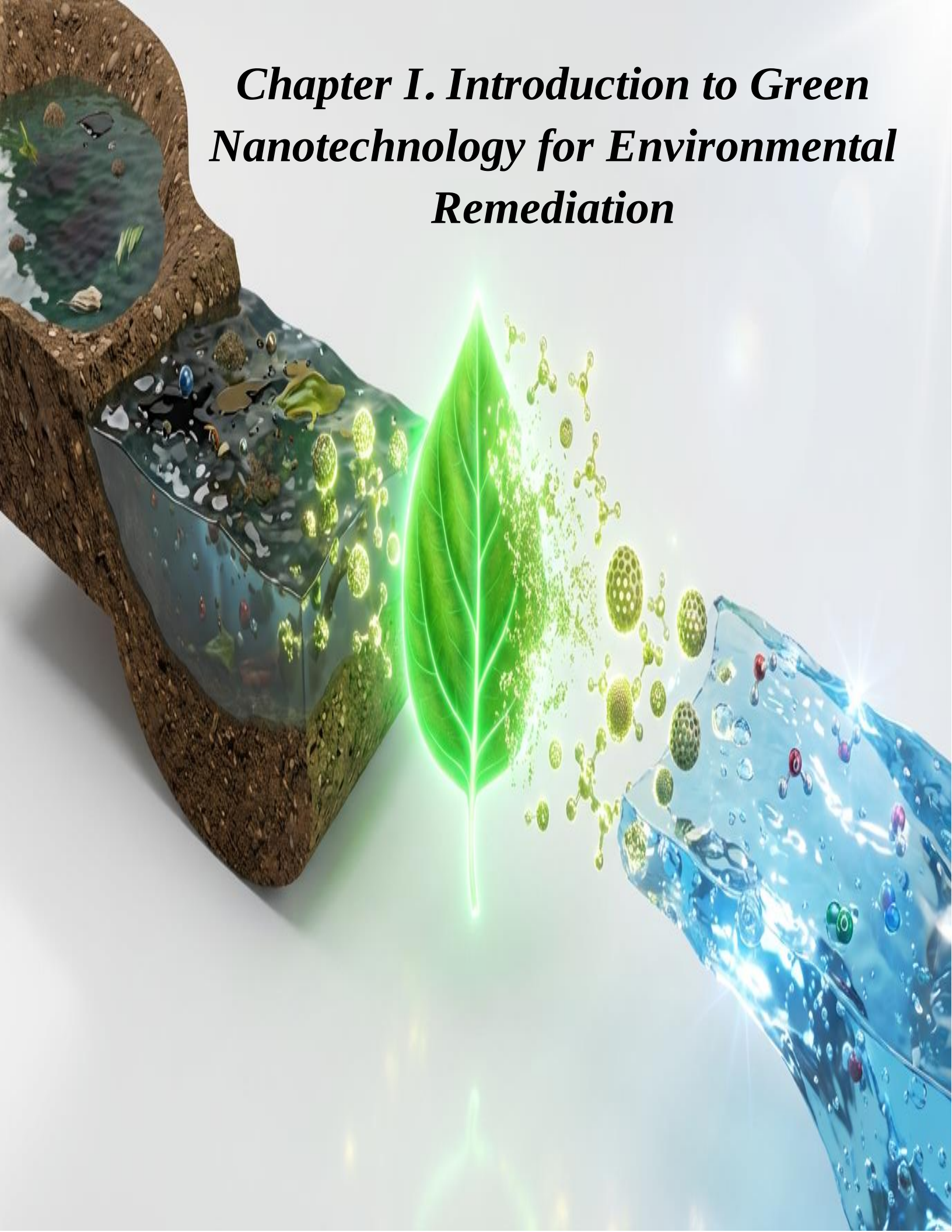

I.1 Water Pollution and Environmental Challenges

Industrial development and rapid population growth have significantly increased global water contamination. Industrial effluents, particularly those generated by the petroleum and textile industries, release substantial quantities of hazardous pollutants into aquatic ecosystems[16]. These pollutants include highly toxic heavy metals (such as Pb^{2+}, Cd^{2+}, Cr^{6+}, Ni^{2+}, and As^{3+}), complex hydrocarbons, oils, and persistent organic dyes [2,3,4,5].

I.1.1 The Global Water Crisis and Industrialization

The global water crisis stands as one of the most formidable challenges of the 21st century, deeply intertwined with the unprecedented rate of global industrialization, relentless population growth, and hyper-urbanization[17]. Freshwater resources, which constitute merely 2.5% of the Earth's total water volume, are under severe stress, with industrial activities consuming a massive fraction of this irreplaceable resource[18]. Aquatic ecosystems, which serve as the fundamental base for both human survival and ecological balance, are continuously exposed to billions of tons of untreated or partially treated industrial effluent discharges annually[19]. Major industrial sectors specifically petroleum refining, textile manufacturing, metallurgy, and heavy chemical production are universally recognized as the primary contributors to this catastrophic level of water contamination[16]. These industries relentlessly discharge a highly complex and heterogeneous matrix of recalcitrant pollutants, including persistent organic pollutants (POPs), synthetic dyes, and heavy metals, directly into freshwater bodies and marine environments[20]. This continuous influx not only devastates local aquatic biodiversity but also severely disrupts the global hydrological cycle, ultimately presenting an existential threat to global environmental sustainability and public health security[21]. To contextualize the scale of this issue, a visual representation of these diverse global water pollution sources is illustrated in **Figure I.1**.

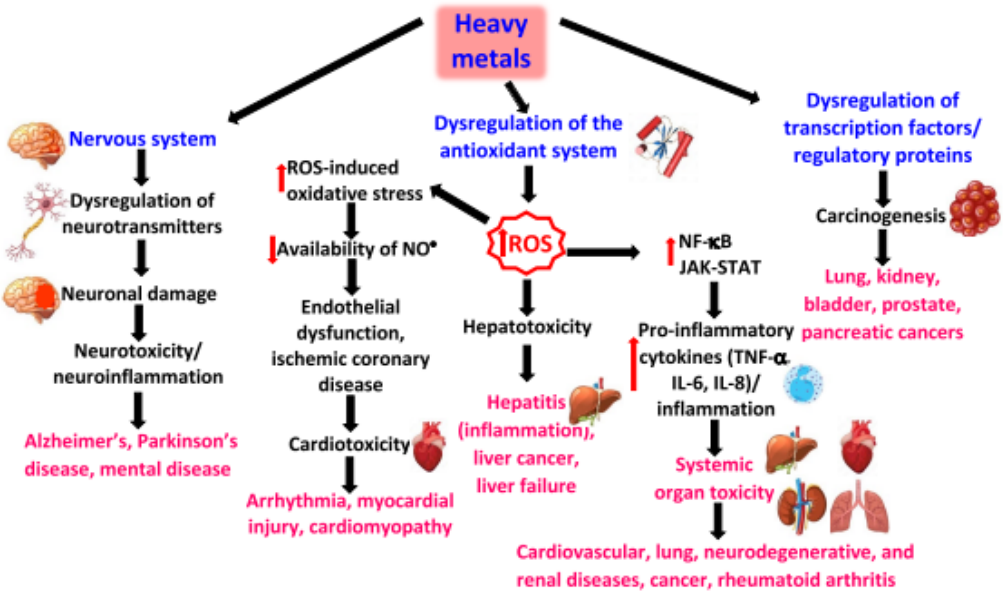

Figure I.1: A simplified view of the mechanisms of heavy metal toxicity and subsequent cellular and organ damage (Adapted from [22]).

To further understand the scale of this environmental crisis, it is essential to categorize the specific pollutants generated by different industries. A detailed summary of the primary industrial sectors and their characteristic recalcitrant effluents is presented in **Table I.1**.

Table I.1: Major industrial sectors and their characteristic recalcitrant water pollutants.

Industrial Sector	***Primary Contaminants in Effluent***	***Environmental Impact***
Petroleum Refining	Total Petroleum Hydrocarbons (TPH), BTEX, PAHs, Heavy metals	High toxicity, formation of oil-in-water emulsions, oxygen depletion
Textile Manufacturing	Synthetic organic dyes, salts, surfactants, heavy metal mordants	Blocking sunlight penetration, halting aquatic photosynthesis
Metallurgy & Mining	Extreme concentrations of heavy metals (Pb^{2+}, Cd^{2+}, As^{3+}, Cr^{6+}), acids	Severe bioaccumulation, pH alteration, extreme toxicity
Chemical Production	Solvents, phenols, persistent organic pollutants (POPs)	Long-term environmental persistence, mutagenic effects

I.1.2 Toxicity of Heavy Metals and Organic Dyes

The persistence and dual toxicity of heavy metals and synthetic organic dyes in petroleum effluents necessitate a profound understanding of their individual chemical behaviors and physiological impacts[20]. In the context of this study, several priority heavy metals are identified due to their dangerous prevalence in industrial discharges [8, 5]. At the molecular level, the profound toxicity of these inorganic pollutants is primarily driven by their strong binding affinity for the sulfhydryl (-SH) groups of essential cellular enzymes and structural proteins, leading to severe conformational changes and enzymatic inhibition[20]. Furthermore, as comprehensively illustrated in Figure 1.1, these metals frequently induce the generation of destructive Reactive Oxygen Species (ROS) through Fenton-like intracellular reactions. This precipitates intense oxidative stress that severely disrupts the antioxidant system, ultimately culminating in neurotoxicity, hepatotoxicity, and the dysregulation of transcription factors leading to various forms of carcinogenesis[23]. Among the most hazardous systemic toxins, lead (Pb^{2+}) enters the environment primarily through industrial activities such as battery manufacturing and petroleum refining[24]. Once ingested, it mimics essential divalent cations like calcium, enabling it to cross the highly selective blood-brain barrier, leading to severe neurological damage, cognitive impairment, and chronic kidney disease [5]. Similarly, cadmium (Cd^{2+}) is highly mobile in aquatic systems and is officially classified as a human carcinogen[25]. Long-term exposure to cadmium, even at trace levels, leads to its bioaccumulation in the renal cortex, causing irreversible kidney dysfunction and "Itai-Itai" disease, characterized by severe bone demineralization and fractures [5]. Furthermore, arsenic (As^{3+}/As^{5+}) is notorious for its acute and chronic toxicity, disrupting cellular metabolism by inhibiting essential enzymes, whereby chronic ingestion is inextricably linked to multi-organ failure and various forms of skin, lung, and bladder cancers [5]. Lastly, while Chromium (III) is an essential trace nutrient, hexavalent chromium (Cr^{6+}) is highly toxic, soluble, and mutagenic[26]. Widely used in stainless steel production and tanning, its high solubility in water allows it to easily penetrate biological phospholipid membranes, causing severe respiratory issues and permanent DNA strand breaks [5]. Concurrently, the discharge of synthetic organic dyes such as Methylene Blue and Rose Bengal into aquatic ecosystems introduces a severe, albeit mechanistically different, ecological disruption [3,4]. Characterized by complex, highly stable aromatic structures, these dyes are chemically engineered to resist biological degradation, thermal variations, and light-induced fading[27]. Even

at minute trace concentrations, they impart intense, persistent coloration to the water column [5]. This artificial chromaticity significantly increases water turbidity and drastically blocks the penetration of incident solar photons[15]. Consequently, the photosynthetic activity of benthic and pelagic aquatic flora is completely halted, triggering a cascading ecological failure[28]. The cessation of photosynthesis leads to a severe depletion of Dissolved Oxygen (DO) levels, rapidly establishing hypoxic conditions that cause the immediate suffocation of aquatic fauna [2,5]. Moreover, the partial, uncontrolled breakdown of these complex dye molecules in nature often generates toxic aromatic amines and intermediate metabolites that are significantly more mutagenic and carcinogenic than the parent compounds, thereby reinforcing the urgent need for advanced, non-selective nanotechnology capable of achieving total mineralization of both organic and inorganic pollutants simultaneously [3, 8, 5].

I.2 Petroleum Wastewater and Industrial Effluents

Petroleum wastewater represents one of the most complex, hazardous, and structurally intricate industrial waste streams to manage globally[29]. Generated extensively during crude oil extraction, refining processes, and petrochemical manufacturing, this wastewater is not a simple solution but a highly stable multiphase colloidal system[30]. It is typically composed of a recalcitrant mixture of dissolved organic compounds, total petroleum hydrocarbons (TPH), emulsified oil droplets, and elevated concentrations of heavy metals [4, 8, 5]. Traditional wastewater treatment methodologies exhibit significant limitations in completely eradicating these diverse contaminants, often suffering from high operational costs, the generation of toxic secondary sludge, and an inherent inability to achieve the total mineralization of complex organic molecules [8,5]. The physical structure of these highly stable oil in water emulsions, specifically the critical orientation of surfactant molecules around the oil droplets, is visually detailed in **Figure I.2**

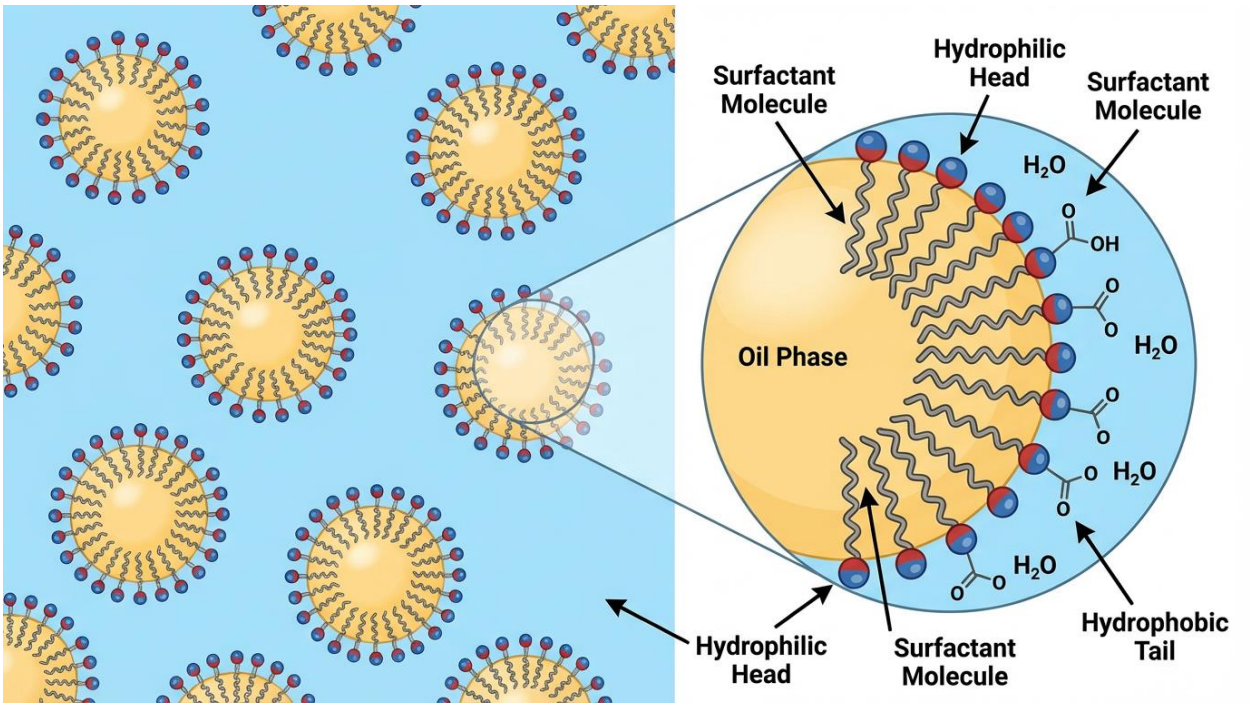

Figure I.2: Schematic representation of an oil-in-water (OIW) emulsion droplet stabilized by amphiphilic surfactant molecules, illustrating the orientation of hydrophilic heads and hydrophobic tails.

I.2.1 Complex Composition of Petroleum Effluents

The chemical profile of this industrial effluent is dominated by a highly recalcitrant organic fraction, primarily consisting of Total Petroleum Hydrocarbons (TPH) [4]. The most concerning environmental fraction includes monocyclic aromatics, such as Benzene, Toluene, Ethylbenzene, and Xylenes (BTEX), alongside Polycyclic Aromatic Hydrocarbons (PAHs) [4]. These hydrocarbons are particularly notorious due to their extreme hydrophobicity, environmental persistence driven by the thermodynamic stability of their delocalized π-electron systems, and well-documented mutagenic properties[31]. When discharged into aquatic ecosystems, they form impermeable lipophilic films on the water surface and readily penetrate the biological phospholipid membranes of marine life, causing severe genetic mutations, enzymatic inhibition, and mass mortality [4]. Beyond dissolved chemical toxicity, the physical state of petroleum effluents presents a formidable remediation challenge largely due to the presence of Oil-in-Water (OIW) emulsions [8]. Unlike free-floating oil that undergoes natural gravity separation, emulsified oil consists of microscopic droplets dispersed homogeneously throughout the water column[32].

These micro-droplets are highly stabilized by natural amphiphilic surfactants, surface-active asphaltenes, and naphthenic acids inherent in crude oil[33]. By forming a rigid steric and viscoelastic interfacial film around the oil droplets, these molecules significantly lower interfacial tension and create strong electrostatic repulsion forces often characterized by a highly negative zeta potential that effectively prevent droplet coalescence, rendering conventional mechanical gravity separation entirely ineffective [8]. Compounding this physical complexity is the elevated concentration of Total Suspended Solids (TSS), which encompasses fine particulate matter such as clay, silica, and precipitated heavy metal complexes [3, 5]. These suspended micro-particles not only increase water turbidity thereby completely blocking sunlight penetration and disrupting aquatic photosynthesis but also act as highly effective toxic carriers[33]. Hazardous organic compounds and heavy metal ions readily adsorb onto their porous surfaces, facilitating the widespread transport and toxic sedimentation of pollutants into the benthic zones of water bodies [3, 5]. The cumulative environmental impact of these massive organic and particulate loads is quantitatively reflected in exceptionally high Chemical Oxygen Demand (COD) levels, indicating a severe concentration of non-biodegradable organic matter that rapidly depletes dissolved oxygen upon microbial degradation, inevitably leading to hypoxic or completely anoxic conditions and the formation of irreversible ecological dead zones [8].

I.2.2 Limitations of Traditional Treatment Methods

Historically, the petroleum industry has relied on a series of conventional wastewater treatment methodologies including chemical coagulation, sand filtration, and biological bioreactors to mitigate environmental impact[34]. However, these traditional techniques exhibit severe operational and economic limitations when confronted with such chemically recalcitrant and physically stable effluents[35]. Chemical precipitation and coagulation require the continuous addition of massive quantities of chemical coagulants, which inevitably generates huge volumes of highly toxic secondary chemical sludge that poses its own severe disposal challenges. Furthermore, while traditional bioreactors utilize microbial communities to degrade organic waste, the exceedingly high concentrations of heavy metals and toxic hydrocarbons frequently induce "microbial shock," effectively poisoning and decimating the active biomass [2, 5]. Additionally, conventional membrane technologies, such as reverse osmosis, are highly susceptible to severe

fouling by emulsified oils and suspended solids, leading to drastic drops in water flux and necessitating frequent, costly membrane replacements[36]. This stark reality highlights the absolute inadequacy of conventional processes in achieving total remediation, forcing the scientific community to pivot urgently toward advanced, high-efficiency nanotechnology alternatives[37].

I.3 Nanotechnology in Environmental Remediation

Nanotechnology has emerged as a revolutionary multidisciplinary field providing highly advanced solutions for environmental pollution control, successfully overcoming the thermodynamic and kinetic limitations of conventional macroscopic techniques [2, 3]. By engineering materials at the nanoscale (typically ranging strictly between 1 and 100 nm), the classical laws of Newtonian physics break down, fundamentally altering the inherent thermodynamic, physical, and chemical characteristics of the substance[38]. At this ultra-small scale, nanomaterials exhibit an exponentially increased surface-area-to-volume ratio, possessing unsaturated coordination sites and inherently high surface free energy [4,8]. This unique structural topology transforms macroscopic oxides into exceptionally reactive materials with tunable optical band gaps and powerful electron-transfer capabilities[39]. Consequently, highly reactive metal oxide nanoparticles specifically ZnO, α-Fe_2O_3, CuO, MgO, and SnO_2 become ideal candidates for the aggressive remediation of complex petroleum effluents[13, 5]. In wastewater treatment, these nanostructured semiconductors operate through highly efficient dual mechanisms: the rapid electrostatic chemisorption of toxic heavy metal cations and the advanced photocatalytic degradation of organic pollutants [2, 8]. Under light irradiation, photo-induced charge separation creates Reactive Oxygen Species (ROS), such as potent hydroxyl radicals (OH) and superoxide anion radicals (O_2^-), which non-selectively attack and cleave the stable chemical bonds of persistent organic hydrocarbons and synthetic dyes, completely mineralizing them into harmless end products [13, 4].

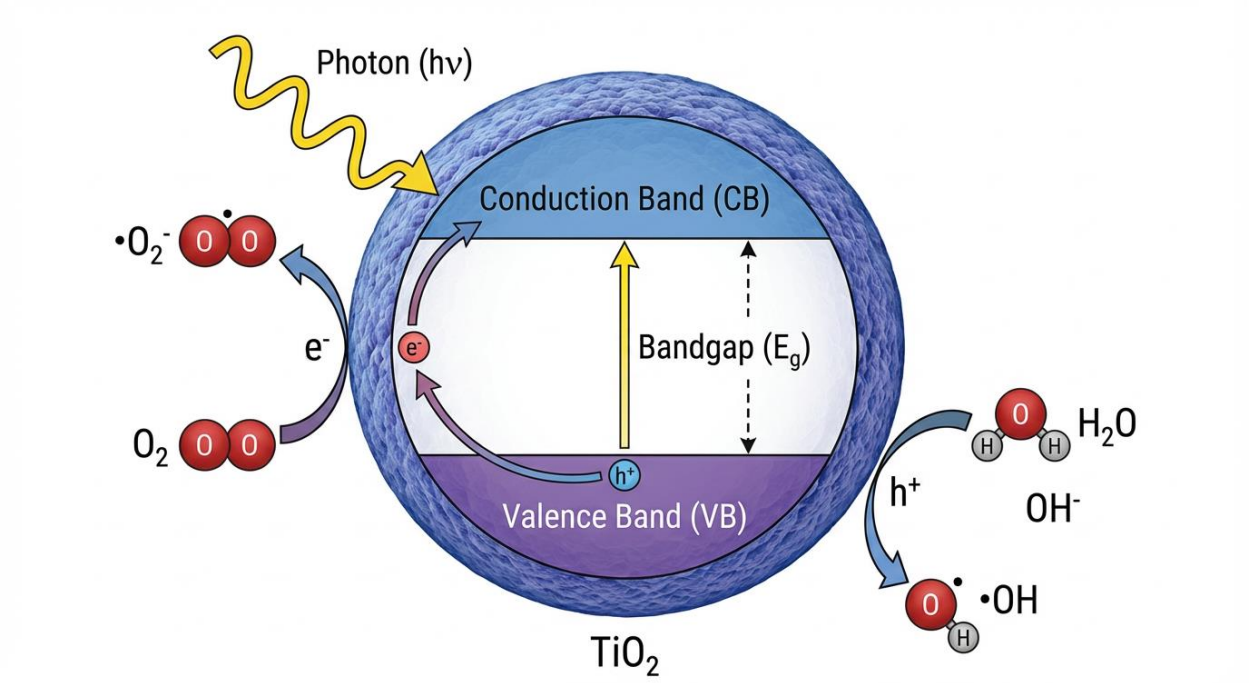

Figure I.3: Schematic illustration of the photocatalytic mechanism of Titanium Dioxide (TiO_2) acting as a general model for semiconductor metal oxide nanoparticles under light irradiation.

The diagram details the generation of photoinduced electron hole pairs and the subsequent production of Reactive Oxygen Species To rigorously evaluate the success of these mechanisms and the structural integrity of the synthesized nanoparticles, a comprehensive suite of advanced analytical techniques is systematically employed. X-ray Diffraction (XRD) and Scanning Electron Microscopy (SEM) determine the crystallographic structure, phase purity, and surface morphology, while Fourier Transform Infrared (FTIR) and Ultraviolet-Visible (UV-Vis) spectroscopy identify specific bioactive functional groups and calculate the critical optical band gap energy [2, 4, 5]. Furthermore, post-treatment analyses, including significant shifts in FTIR absorption bands and elemental mapping via Energy Dispersive Spectroscopy (EDS), provide definitive confirmation of the targeted heavy metals successfully sequestered and immobilized onto the surface of the biogenic nanoparticles [3, 5].

I.4 Green Synthesis of Nanomaterials

While traditional physical and chemical methodologies such as sol-gel processes, chemical vapor deposition, and co-precipitation have been extensively utilized for nanoparticle synthesis, they are increasingly scrutinized due to their severe environmental and economic drawbacks[40]. These conventional techniques typically demand high energy inputs, extreme localized temperatures, and, most critically, the extensive use of highly toxic, hazardous capping agents and chemical reductants (e.g., sodium borohydride, hydrazine hydrate)[41]. The inevitable generation of toxic chemical byproducts sharply contradicts the global imperative for environmental sustainability and limits the biocompatibility of the synthesized nanomaterials for sensitive ecological applications [13], [8]. In stark contrast, the "Green Synthesis" paradigm has emerged as a revolutionary, eco-friendly, and highly sustainable alternative, strictly adhering to the foundational principles of Green Chemistry[38]. Among various biological templates (including bacteria, fungi, and algae), plant-mediated (phytogenic) synthesis stands out as the most advantageous methodology[42]. It completely eliminates the need for pathogenic microbial cultures, avoids complex and time-consuming intracellular maintenance, and offers rapid, scalable, and cost-effective production under ambient thermodynamic conditions [2, 5].

I.4.1 Role of plant extract

The profound efficacy of plant extracts in the synthesis of metal oxide nanoparticles lies in their rich, highly complex biochemical composition[43]. Aqueous plant extracts are naturally abundant in an array of highly active secondary metabolites, collectively termed phytochemicals, which include polyphenols, flavonoids, alkaloids, terpenoids, and phenolic acids [4,8]. During the synthetic process, these phytochemicals perform a critical, dual-functional synergistic role[44]. The hydroxyl (-OH) and ketonic functional groups present in compounds like flavonoids possess strong electron-donating capabilities[45]. They rapidly reduce the high-oxidation-state metal cations present in the aqueous precursor salt solutions down to their zero-valent or lower-oxidation-state nanostructured forms[46]. Following this instantaneous bio-reduction phase, a profound secondary mechanism occurs: steric stabilization[47]. The bulky biological molecules and unreacted organic ligands from the plant extract immediately self-assemble and tightly bind to the highly reactive surface of the newly formed nanoparticles[48]. By forming a robust, biological capping layer, they induce significant steric hindrance and electrostatic repulsion[49]. This

effectively prevents the highly energetic nanoparticles from undergoing spontaneous thermodynamic agglomeration (Ostwald ripening), thereby dictating their final morphological shape, controlling their crystallite size, and ensuring prolonged structural stability in aqueous suspensions [3, 5]. Consequently, the resulting biogenic nanoparticles are not only structurally highly stable but also inherently bio-functionalized, enhancing their surface reactivity and selective binding affinity for targeted pollutant remediation[50].

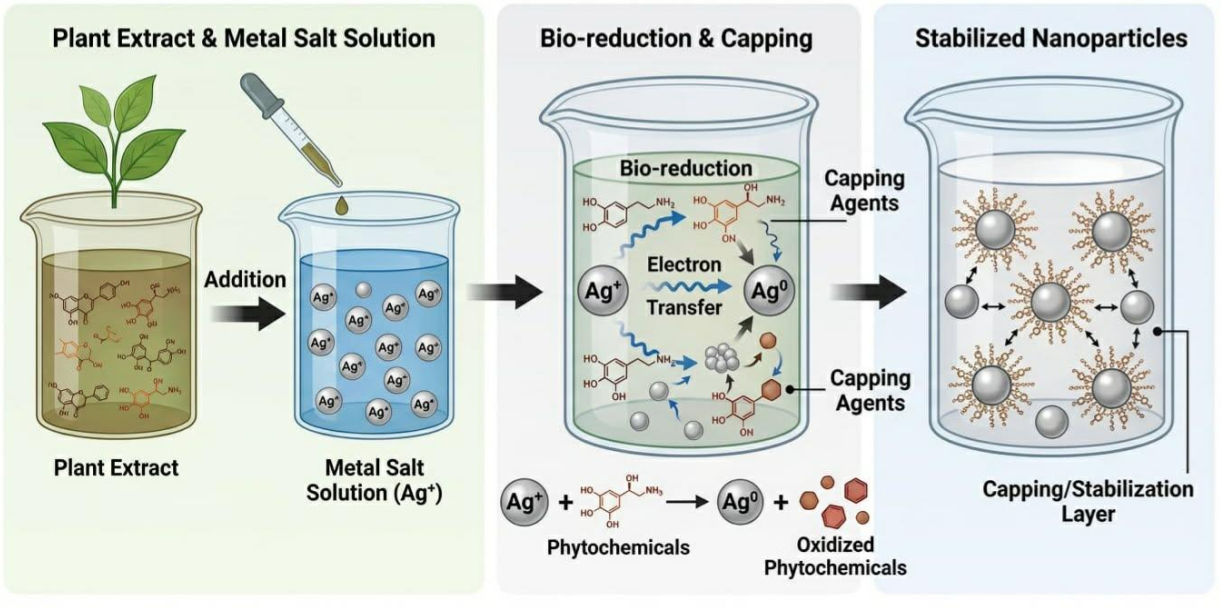

Figure I.4: Schematic illustration of the plant-mediated green synthesis of nanomaterials.

I.4.2 Eco-friendly synthesis of nanoparticles

The efficacy of plant-mediated synthesis in producing metal oxide nanocomposites stems from the phytochemical composition of the aqueous extracts used as reducing and stabilizing agents [2, 3]. These bioactive compounds including flavonoids, polyphenols, phenolic acids, and terpenoids possess hydroxyl (-OH) and carbonyl (C=O) functional groups with exceptional electron-donating capabilities [13, 4]. During synthesis, these phytochemicals perform a critical dual role: they act as reducing agents by donating electrons to metal cations (Fe^{3+}, Cu^{2+}, Zn^{2+}, Mg^{2+}, Sn^{2+}), converting them to nanostructured oxides, and subsequently form a protective capping layer around the newly formed nanoparticles that prevents agglomeration through steric hindrance and electrostatic repulsion [2, 8, 5]. The specific phytochemical profiles of the plant extracts utilized in the six studies demonstrate this principle clearly. Pistacia lentiscus extract, rich in flavonoids, facilitated the biosynthesis of $MgO@SnO_2$ nanocomposites with uniform particle size (~25 nm) [2]. Mentha

pulegium extract, with its high phenolic content (124.27 mg GAE/g), enabled the synthesis of ZnO@CuO and Ca/α-Fe_2O_3/ZnO/CuO nanocomposites with remarkable crystallinity [13, 8]. Laurus nobilis extract successfully mediated the formation of Fe_3O_4 nanoparticles and their subsequent coating with chitosan and silver [3, 4], while Portulaca oleracea extract and pure gallic acid enabled the controlled synthesis of α-Fe_2O_3, CuO, ZnO nanoparticles [5]. FTIR analysis confirms this phytochemical involvement, consistently showing the disappearance of O-H (3200-3600 cm^{-1}) and C=O (1700-1750 cm^{-1}) peaks after synthesis indicating their participation in metal ion reduction alongside the appearance of new metal-oxygen peaks in the 400-800 cm^{-1} region confirming nanoparticle formation [2, 3, 8]. Furthermore, the adsorbed phytochemicals impart enhanced surface reactivity, as evidenced by zeta potential measurements showing excellent colloidal stability (-29.06 mV for Ca/α-Fe_2O_3/ZnO/CuO and +18.9 mV for CS/Fe_3O_4) [13, 3]. Several factors influence this synthesis process, including phytochemical concentration, pH, temperature (70-85°C), and reaction duration (2-3 hours), all of which affect reduction rate, nucleation kinetics, and final nanoparticle properties [2,5].

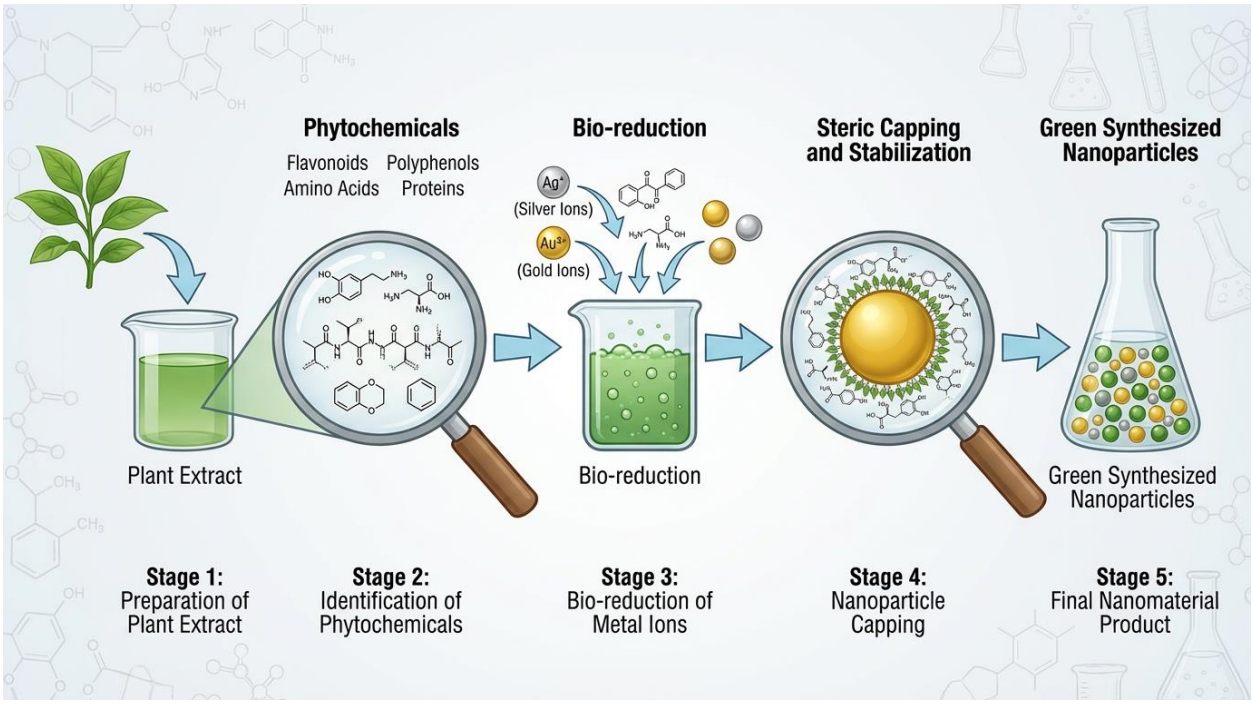

Figure I.5: Comprehensive five-stage schematic representation of the plant-mediated green synthesis process**.**

I.4.3 Characterization Techniques of Nanomaterials

In the systematic characterization of synthesized nanomaterials, identifying the specific biogenic precursors is fundamental to understanding their final structural and chemical properties[51]. For instance, the aqueous extracts of *Mentha pulegium* and *Portulaca oleracea* have demonstrated exceptional efficacy in the fabrication of highly pure single metal oxides such as α-Fe_2O_3, CuO, and ZnO, as well as complex multimetallic systems designed for the remediation of contaminated sludge and petroleum effluents [13,8,5]. Similarly, extracts from *Pistacia lentiscus* and *Laurus nobilis* have been widely utilized to synthesize robust matrices like MgO@SnO_2 and magnetic Ag@Fe_3O_4 nanocomposites, conferring both superior photocatalytic efficiency and notable antibacterial properties [2, 3, 4]. Furthermore, the integration of natural biopolymers, specifically Chitosan extracted from crustacean shells, offers a significant structural advantage by providing a non-toxic capping matrix rich in amine (-NH_2) and hydroxyl (-OH) functional groups [3], which act as powerful biological chelating agents to maximize heavy metal capture.

To scientifically validate the successful formation, structural integrity, and functional surface properties of all these diverse plant-mediated nanomaterials, a specific set of advanced analytical techniques must be systematically employed [2**,** 5]. These essential characterization methods are visually represented in **Figure I.6**.

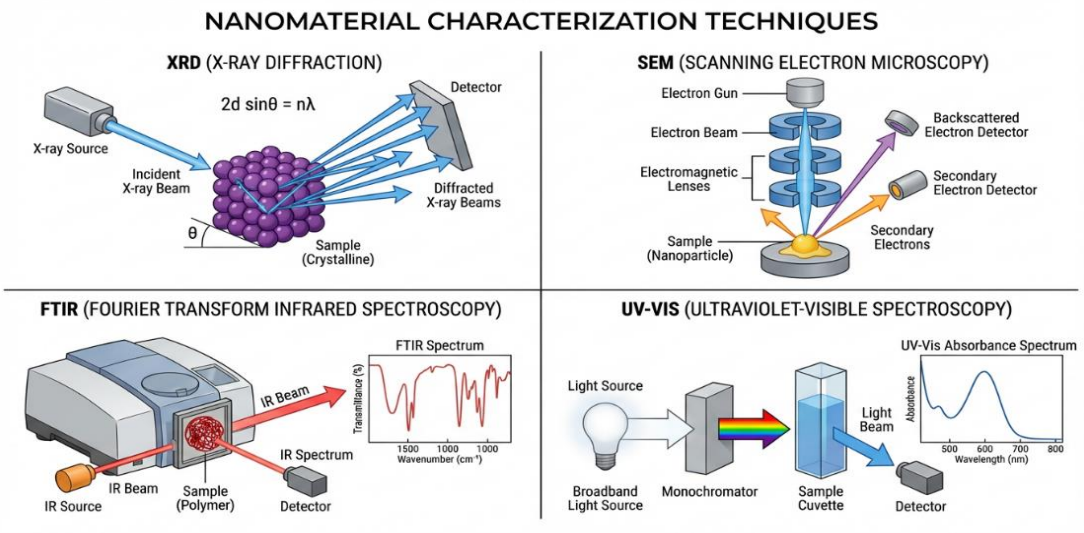

Figure I.6: Schematic representation of various characterization techniques (XRD, SEM, FTIR, UV-Vis) utilized to analyze the physicochemical properties of synthesized nanomaterials**.**

To provide a comprehensive technical overview, the diverse natural precursors used in these studies, along with the successfully synthesized metal oxide nanoparticles and their targeted pollutants, are systematically categorized in **Table I.2**.

Table I.2: Comprehensive summary of plant-mediated nanomaterials, active phytochemicals, and their heavy metal removal applications.

Plant Extract Source	*Plant Part Used*	*Major Phytochemicals*	*Synthesized Nanoparticles*	*Target Heavy Metal*	*Reference*
***Pistacia lentiscus* leaves**	Leaves	Phenols, Alcohols	MgO@SnO_2@PVP NCs	Cr, Mo, Sb, Pb, Cd, Zn	[2]
***Mentha pulegium L.* leaves**	Leaves	Phenols, Flavonoids	Ca/α-Fe_2O_3/ZnO/CuO NCs	Pb, Zn, Se, Cr, Cu, Ni	[13]
***Laurus nobilis* & Shrimp shells**	Leaves & Shrimp Shells	Phenols, Chitosan	CS/Fe_3O_4 NCs	As, Be, Cd, Cr, Mn, Ni, Pb	[3]
***Laurus nobilis* leaves**	Leaves	Polyphenols, Flavonoids	Ag@Fe_3O_4 NCs	As, Cd, Cr, Mn, Mo, Ni, Pb	[4]
***Mentha pulegium L.* leaves**	Leaves	Phenols, Amines, Proteins	ZnO@CuO NCs	As, Bi, Cd, Cr, Ni, Pb, Zn	[8]

Plant Extract Source	*Plant Part Used*	*Major Phytochemicals*	*Synthesized Nanoparticles*	*Target Heavy Metal*	*Reference*
***Portulaca oleracea* leaves**	Leaves	Alcohols, Aldehydes, Acids	α-Fe_2O_3, CuO, ZnO NPs	As, Bi, Cd, Cr, Mn, Ni, Pb, Zn	[5]

I.5 Applications of Nanocomposites in Wastewater Treatment

While single metal oxide nanoparticles are highly effective, engineering nanocomposites that combine multiple metal oxides or integrate functional polymers drastically enhances overall remediation performance[52]. The synergistic effects within multimetallic structures (such as ZnO@CuO or Ca/α-Fe_2O_3/ZnO/CuO) or biopolymer-coated magnetic cores (like CS/Fe_3O_4) lead to vastly improved adsorption capacities and extended photocatalytic endurance [13, 3, 8]. These advanced nanocomposites possess the unique capability to simultaneously target and remove diverse classes of pollutants from a single effluent stream[53]. They efficiently sequester heavy metals via electrostatic attraction, catalytically break down long-chain hydrocarbons and persistent dyes, and reduce chemical oxygen demand (COD) and total suspended solids (TSS) simultaneously [3, 4, 8, 5]. Furthermore, the integration of magnetic cores ensures the rapid and energy-efficient separation of the spent nanomaterials from the purified water [3, 4].

I.5.1 Metal Oxide Nanoparticles in Water Treatment

The construction of multimetallic nanocomposites represents a significant advancement in designing high-performance materials for wastewater treatment [13,8]. Single metal oxide nanoparticles, despite their promising properties, face practical limitations including rapid electron-hole pair recombination, saturation of active surface sites, and agglomeration in aqueous media [2, 4]. The strategic integration of multiple metal oxides into a single engineered matrix

overcomes these limitations through synergistic effects that amplify overall remediation performance[3,5].

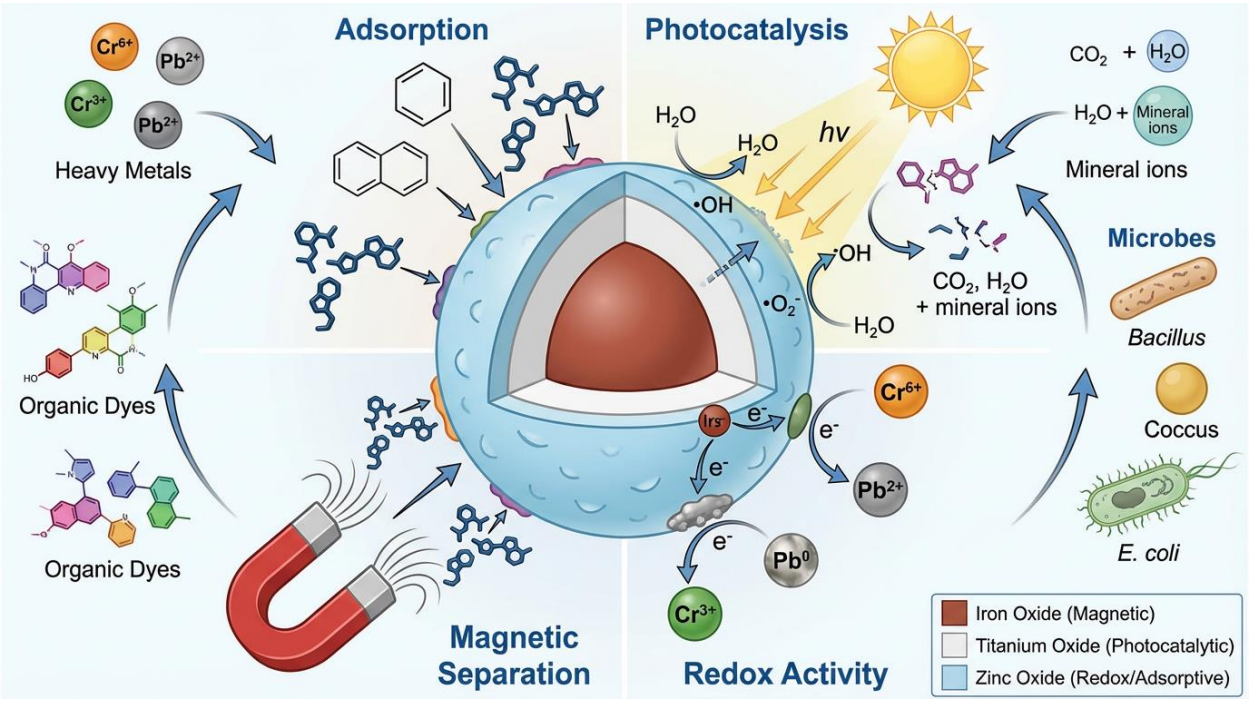

Figure I.7: Schematic representation of synergistic effects in multimetallic nanocomposites for wastewater treatment.

This principle manifests distinctly across the multimetallic systems reviewed. The binary MgO@SnO_2 nanocomposite (Article 1) harnesses the strong basicity and high surface area of MgO alongside the wide bandgap and photocatalytic activity of SnO_2, enabling simultaneous heavy metal adsorption and hydrocarbon degradation under sunlight [2]. The quaternary Ca/α-Fe_2O_3/ZnO/CuO system (Article 2) exemplifies functional complementarity: CaO provides alkalinity and ion-exchange capacity, α-Fe_2O_3 contributes redox activity, ZnO drives photocatalytic reactions, and CuO enhances electron transfer and metal selectivity [13]. This compositional diversity yielded removal efficiencies of 84.1% for lead, 74.6% for zinc, and 73.7% for chromium from contaminated sludge [13].

I.5.2 Magnetic Separability and Sustainable Reuse

The incorporation of magnetic cores, particularly Fe_3O_4, addresses one of the most persistent challenges in practical wastewater treatment: recovering spent nanomaterials without secondary pollution [3,4]. Conventional powder-based systems struggle with this separation step, often

requiring energy-intensive centrifugation or filtration that risks nanoparticle release into treated water [4]. Magnetic hybridization resolves this through simple, rapid separation using external magnetic fields [3, 5]. The CS/Fe_3O_4 and Ag@Fe_3O_4 nanocomposites (Articles 3 and 4) exemplify this approach, exhibiting superparamagnetic behavior that enables efficient magnetic separation while maintaining excellent colloidal stability during treatment [3, 4]. This recoverability extends beyond separation to enable multiple treatment cycles, fundamentally enhancing process economics[54]. MgO@SnO_2@PVP maintained degradation efficiency over five successive cycles, with minimal decline from 88.13% to 86.98% for oily wastewater and from 85.54% to 83.87% for total suspended solids [2]. XRD analysis confirmed preservation of crystalline structure throughout repeated use, demonstrating structural integrity [2]. Similarly, Ag@Fe_3O_4 retained photocatalytic activity for rose bengal degradation over five cycles, decreasing marginally from 96.8% to 94.6% [4], while ZnO@CuO showed comparable stability with efficiency dropping from 100% to 97.12% for OIW over five cycles [8].

I.5.3 Adsorption Equilibrium and Kinetics

To accurately describe the interaction between the synthesized nanocomposites and pollutants, the study employs rigorous mathematical models to quantify the distribution of adsorbate molecules at equilibrium. The Langmuir Isotherm Model is utilized to describe a highly homogeneous surface where adsorption occurs as a uniform single monolayer, mathematically expressed as follows [2,3]:

$$qe = \frac{q_m K_L C_e}{1 + K_L C_e}$$

In this context, qe represents the amount of pollutant adsorbed at equilibrium, C_e is the equilibrium concentration, qm is the maximum monolayer adsorption capacity, and K_L is the Langmuir constant. In stark contrast, the Freundlich Isotherm Model characterizes adsorption on highly heterogeneous surfaces, accommodating multilayer formation and exponentially varying binding energies through the following relationship [2,8]:

$$qe = K_f C^{1/n_e}$$

Here, K_f represents the adsorption capacity and $1/n_e$ indicates the intensity of adsorption and surface heterogeneity. From a dynamic perspective, the rate-controlling steps of the overall remediation process are determined using kinetic models, specifically the pseudo-second-order equation [13, 5]:

$$\frac{t}{q_t} = \frac{1}{k_2 q_e^2} + \frac{t}{q_e}$$

In this equation, q_t is the amount adsorbed at time t and k_2 is the rate constant of the pseudo-second-order adsorption. The successful application of these models strongly suggests that the dominant remediation mechanism is chemisorption, primarily driven by direct chemical bonding, electrostatic attraction, and electron exchange between the toxic pollutants and the bio-functionalized surface of the nanomaterial [2, 8, 5].

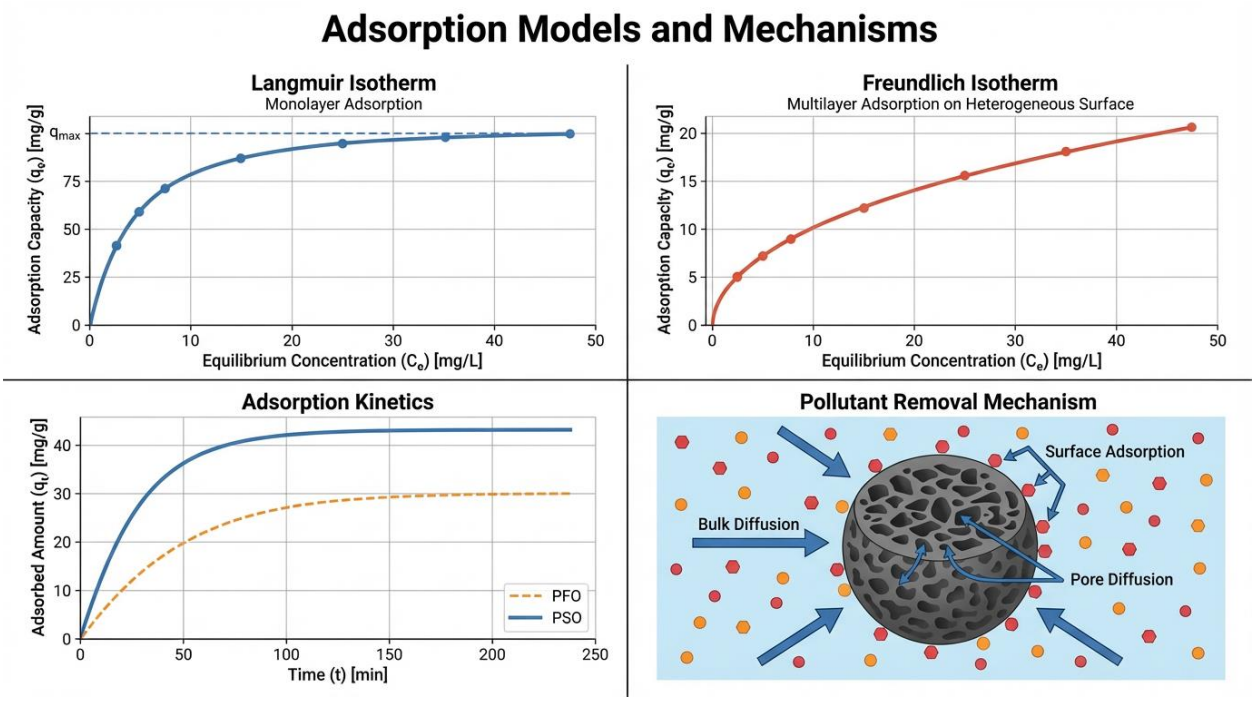

Figure I.8: Graphical representation of classical adsorption isotherms (Langmuir vs. Freundlich) and kinetic models demonstrating the pollutant removal mechanism.

To rigorously comprehend the intrinsic nature of the adsorption process, thermodynamic parameters specifically the standard Gibbs free energy change (ΔG°), enthalpy change (ΔH°), and entropy change (ΔS°) must be evaluated. A negative value of ΔG° fundamentally confirms the spontaneous and thermodynamically feasible nature of the heavy metal adsorption onto the biogenic nanomaterials. Concurrently, the magnitude and sign of ΔH° delineate whether the sequestration process is endothermic or exothermic, while a positive ΔS° value reflects an increased state of randomness and affinity at the solid-solution interface during the immobilization of the metal ions [2, 4, 8].

I.6 Research Gap

While previous literature has extensively discussed the green synthesis of isolated, single-metal oxide nanoparticles, there remains a critical research gap regarding the comprehensive comparative analysis of advanced multimetallic systems. Although a single metal oxide works reasonably well, engineering complex nanocomposites by mixing multiple metal oxides or integrating specific natural polymers boosts the overall performance dramatically. This work uniquely bridges the literature gap by critically evaluating the synergistic effects specifically optical band-gap narrowing and enhanced adsorption kinetics within engineered binary, ternary, and quaternary heterojunctions compared to conventional methods in advanced wastewater treatment.

I.7 Objectives of the Thesis

Based on the critical environmental challenges posed by complex petroleum wastewater and the highly promising, sustainable solutions offered by green nanotechnology, the primary objective of this review thesis is to systematically analyze and synthesize recent pioneering studies on plant-mediated metal oxide nanocomposites. Specifically, this research aims to evaluate the fundamental methodologies and environmental benefits of utilizing natural plant extracts and biopolymers in the green synthesis of advanced nanomaterials [2,5]. Furthermore, the thesis discusses the structural, morphological, and optical characteristics of these biogenic nanomaterials as conclusively confirmed by advanced analytical techniques, including XRD, SEM, FTIR, and UV-Vis spectroscopy. Ultimately, this work seeks to critically analyze the specific removal efficiencies, adsorption isotherms, and kinetic models associated with the elimination of extreme petroleum pollutants, while highlighting the unique synergistic engineering advantages such as magnetic separability and enhanced photocatalytic degradation that position these green-synthesized nanocomposites as superior, sustainable candidates for large-scale industrial wastewater remediation.

Chapter II. Experimental Methods for Nanocomposite Synthesis and Characterization

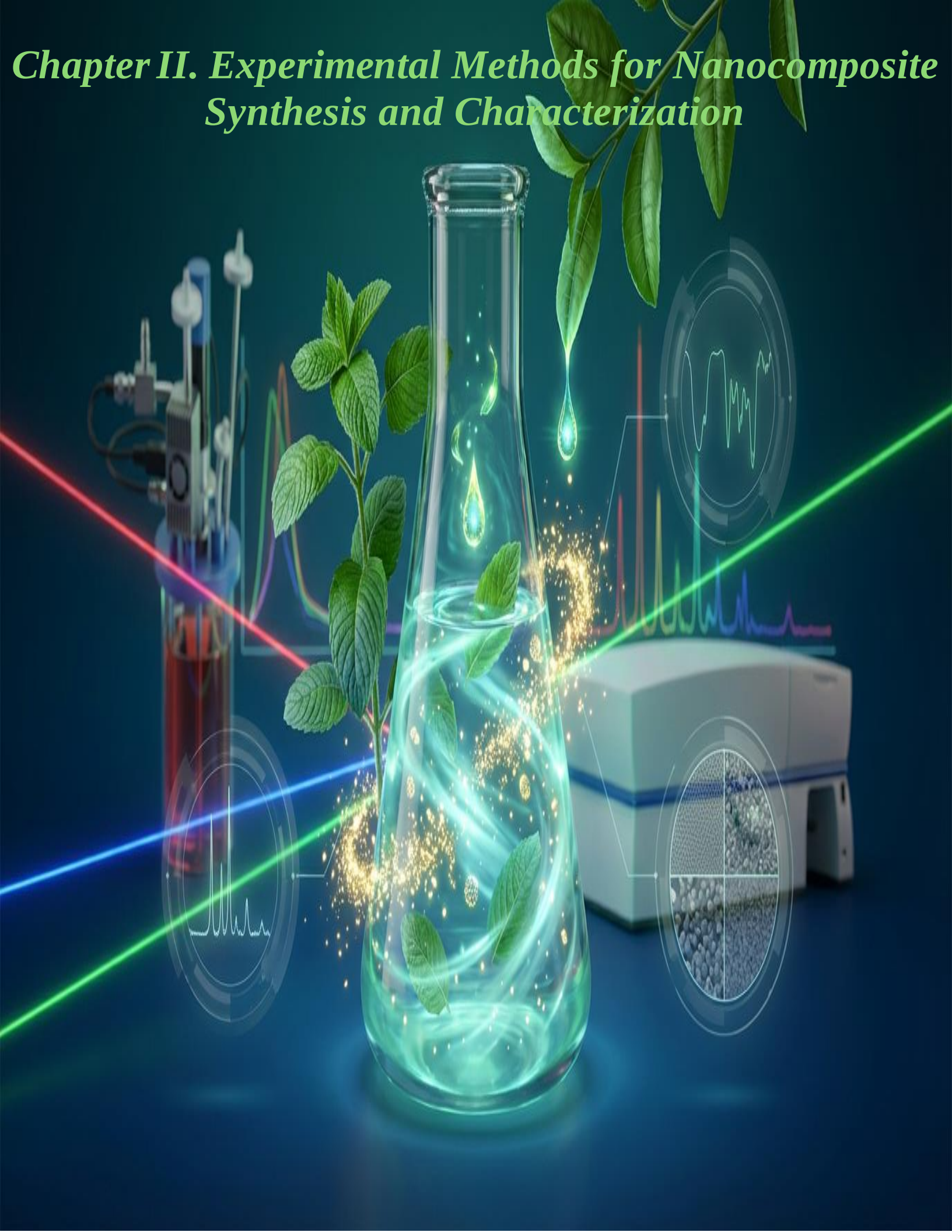

II.1 Materials Used in the Reviewed Studies

The reviewed studies investigated a diverse array of metal precursors, plant extracts, and chemical reagents essential for the green synthesis of high-performance metal oxide nanoparticles and their respective nanocomposites.

II.1.1 Metal Precursors and Chemical Reagents

The core synthesis of the green nanomaterials heavily relied on high-purity analytical grade transition metal salts (typically exceeding 98% purity, supplied by renowned chemical manufacturers such as Sigma-Aldrich or Merck)[55], which served as the primary source of metal cations that undergo biological reduction. Specifically, for the synthesis of ZnO nanoparticles and their nanocomposites, zinc nitrate hexahydrate and zinc acetate dehydrate were predominantly utilized due to their high solubility [8, 5]. Concurrently, the fabrication of iron-based magnetic core nanoparticles critically depended on iron (III) chloride hexahydrate [13, 3, 4, 5]. Furthermore, copper (II) nitrate trihydrate and copper (II) sulfate were strategically employed to generate CuO nanoparticles [8, 5]. Crucially, to synthesize advanced heterojunctions, silver nitrate ($AgNO_3$) was utilized as the primary precursor for the $Ag@Fe_3O_4$ nanocomposite [4], while specific calcium precursors were integrated to formulate the quaternary $Ca/\alpha\text{-}Fe_2O_3/ZnO/CuO$ system [13]. Additionally, complex binary systems like $MgO@SnO_2$ required a precise stoichiometric mixture of magnesium nitrate and tin (II) chloride [2]. Beyond these primary metal salts, auxiliary chemicals were indispensable[56]. Absolute ethanol and double-distilled water were extensively used for rigorous washing protocols[57]. For critical pH adjustments, standard solutions of 0.1 M HCl and 0.1 M NaOH were strictly applied. Finally, biopolymers such as chitosan, extracted from marine shrimp shells, and synthetic polymers like polyvinylpyrrolidone (PVP) were utilized as structural capping and surface-modifying agents to prevent particle agglomeration and enhance surface reactivity [2, 3].

II.1.2 Plant Extracts for Green Synthesis

A pivotal element of the reviewed methodologies was the paradigm shift toward eco-friendly chemistry, where specific plant species were carefully selected to serve as robust, natural biological factories, completely substituting highly toxic and expensive chemical reductants. The botanical

sources extensively investigated included the leaves of *Portulaca oleracea* [5], *Mentha pulegium L.* [13, 8], *Laurus nobilis* [3, 4], and *Pistacia lentiscus* [2]. These specific plants were chosen due to their extraordinary innate biochemical profiles. Their aqueous extracts are heavily concentrated with diverse secondary metabolites and phytochemicals, primarily water-soluble polyphenols, flavonoids, organic acids, aldehydes, and biogenic amines. From a mechanistic perspective, these bioactive functional groups possess high thermodynamic potential; they act simultaneously as powerful electron donors, reducing metal cations to their respective oxide phases, and as excellent steric stabilizers that wrap around the nascent nanoparticles to govern their final morphological growth and prevent unwanted aggregation.

Table II.1: Plant extracts utilized in the reviewed studies and their major phytochemical constituents.

Plant Species	*Major Phytochemicals*	*Nanomaterials Synthesized*	*Reference*
Pistacia lentiscus	Flavonoids, tannins, phenolic acids	$MgO@SnO_2$, $MgO@SnO_2$@PVP	[2]
Mentha pulegium	Polyphenols (124.27 mg GAE/g), flavonoids	ZnO@CuO, Ca/α-Fe_2O_3/ZnO/CuO	[13, 8]
Laurus nobilis	Epicatechin, procyanidins, 1,8-cineole	Fe_3O_4, CS/Fe_3O_4, Ag@Fe_3O_4	[3, 4]
Portulaca oleracea	Alpha-linoleic acid, alpha-tocopherol	α-Fe_2O_3, CuO, ZnO	[5]

II.1.3 Pollutants studied in the reviewed papers

The synthesized bio-nanomaterials were purposefully subjected to rigorous environmental remediation tests, targeting a complex matrix of pollutants strictly defined by the reviewed methodologies. The primary focus was placed on highly toxic and recalcitrant heavy metals, specifically targeting lead (Pb^{2+}), cadmium (Cd^{2+}), chromium (Cr^{6+} and Cr^{3+}), nickel (Ni^{2+}), arsenic (As^{3+}), zinc (Zn^{2+}), copper (Cu^{2+}), antimony (Sb^{3+}), bismuth (Bi^{2+}), manganese (Mn^{2+}), molybdenum (Mo^{2+}), beryllium (Be^{2+}), and selenium (Se^{2-}) [2, 13, 3, 4, 8, 5]. Beyond inorganic

metal ions, the studies extensively evaluated the removal of complex organic and physical contaminants characteristic of industrial and petroleum effluents. These included stable oil-in-water emulsions, monocyclic and polycyclic aromatic hydrocarbons (such as phenolic derivatives) [2, 4, 8, 5], and persistent synthetic organic dyes [3, 4]. Furthermore, to confirm practical industrial applicability, specific studies demonstrated the nanomaterials' efficiency in drastically reducing macroscopic physical pollution indicators, notably Total Suspended Solids (TSS) and Chemical Oxygen Demand (COD) from real petroleum wastewater matrices [4, 8, 5].

Table II.2: Summary of the diverse targeted pollutants removed by the synthesized nanomaterials.

Pollutant Category	*Specific Pollutants*	*References*
Heavy Metals	Pb^{2+}, Cd^{2+}, Cr^{6+}/Cr^{3+}, Ni^{2+}, As^{3+}, Zn^{2+}, Cu^{2+}, Sb^{3+}, Bi^{2+}, Mn^{2+}, Mo^{2+}, Be^{2+}, Se^{2-}	[2, 13, 3, 4, 8, 5]
Organic Pollutants	Oil-in-water emulsions, phenolic compounds, PAHs	[2, 4, 8, 5]
Synthetic Dyes	Methylene Blue, Rose Bengal, Toluidine Blue	[3, 4]
Physical Indicators	Total Suspended Solids (TSS), Chemical Oxygen Demand (COD)	[4, 8, 5]

II.1.4 Real Petroleum Wastewater Characteristics

To bridge the gap between laboratory-scale simulations and real-world industrial applicability, several of the reviewed studies [2, 4, 8, 5] decisively moved beyond synthetic metallic solutions by utilizing actual, raw petroleum wastewater[58]. These effluents were directly sampled from the discharge pipelines of regional petrochemical refineries and oil-gas separation plants[59]. Before any nanomaterial intervention, these raw samples represented a highly complex and severely contaminated aqueous matrix.

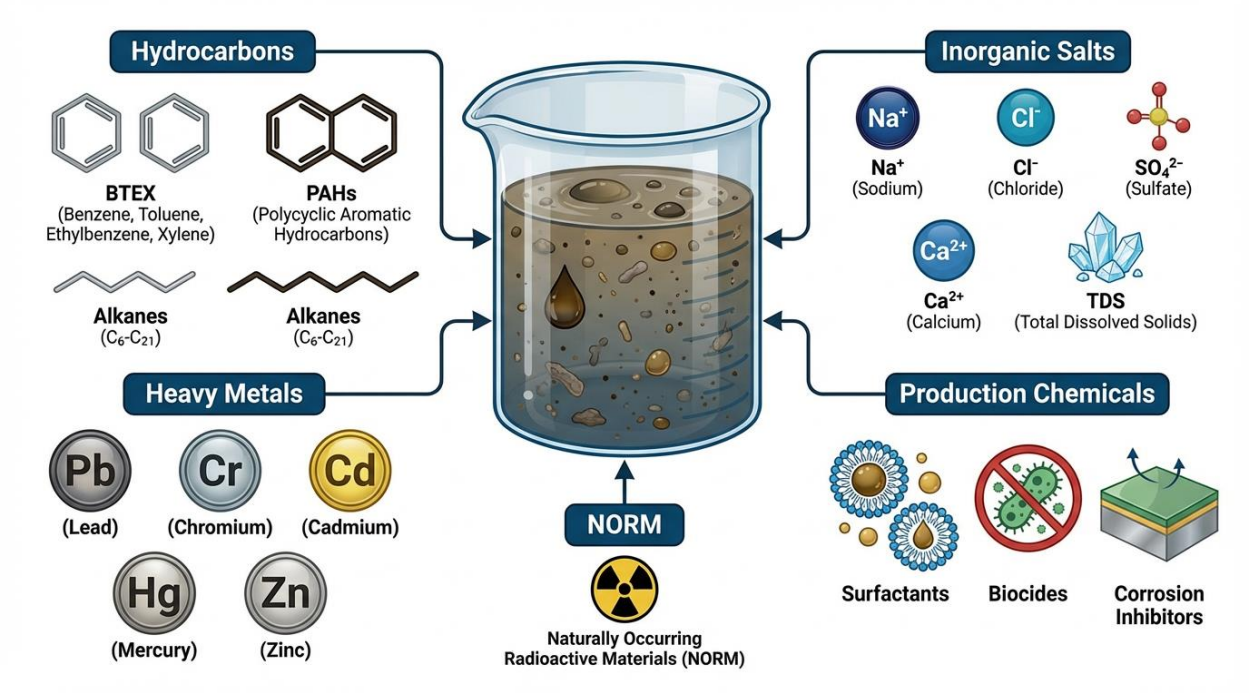

Figure II.1: Schematic representation of the complex composition of raw petroleum wastewater before nanomaterial treatment.

Initial characterizations of the untreated wastewater typically revealed extreme pollution loads, including exceptionally high Chemical Oxygen Demand (COD) indicating massive organic pollution, elevated Biochemical Oxygen Demand (BOD), high concentrations of Total Suspended Solids (TSS), and dense emulsified oil-in-water fractions[8,5]. Furthermore, the raw matrix natively contained trace baseline concentrations of the aforementioned heavy metals, thereby serving as the ultimate stress test to validate the synergistic adsorption and catalytic degradation capabilities of the green-synthesized nanomaterials[2,8].

II.2 Green Synthesis of Metal Oxide Nanoparticles

The development of sustainable, eco-friendly, and cost-effective methodologies for fabricating metal oxide nanomaterials is a primary focus of the reviewed literature. This section outlines the biogenic synthesis approaches, highlighting the critical transition from conventional, hazardous chemical routes to green, plant-mediated processes. The following subsections detail the specific biological agents, synthesis protocols, and precise operating parameters employed to achieve highly crystalline and structurally stable nanocomposites.

Figure II.2: Diagram of the plant-mediated green synthesis process from the initial preparation of the plant extract and identification of active phytochemicals to the final steric stabilization of the biogenic nanoparticles.

II.2.1 Preparation of Aqueous Plant Extracts

The extraction procedures followed a standardized green protocol to maximize the yield of active bioactive compounds. Freshly collected plant leaves (*Portulaca oleracea*, *Mentha pulegium*, *Laurus nobilis*, and *Pistacia lentiscus*) were thoroughly washed with double-distilled water to remove surface impurities, completely shade-dried at room temperature to prevent the thermal degradation of heat-sensitive phytochemicals, and subsequently pulverized into a fine homogenous powder. In a typical extraction process, a precise mass of the plant powder, generally ranging from 10 to 20 g, was dispersed into a specific volume of deionized water, typically 100 mL. The aqueous mixture was continuously magnetically stirred and heated to sub-boiling temperatures ranging between 60 °C and 80 °C for a duration of 1 to 2 hours. Finally, the resulting dark-colored phytochemical broths were cooled to room temperature and filtered using Whatman filter paper to separate the residual biomass, yielding pure aqueous extracts that were utilized immediately for the subsequent nanoparticle synthesis [2, 13, 3, 4, 8, 5].

II.2.2 Synthesis Protocols and Operating Parameters

The reviewed papers successfully established environmentally friendly, cost-effective, and scalable green synthesis routes for producing metal oxide nanoparticles. Typically, the synthesis procedure was initiated by the preparation of the aqueous plant extract. Fresh or dried plant leaves were thoroughly washed, crushed, and boiled in distilled water under controlled conditions to extract the active phytochemicals, followed by careful filtration to isolate the pure biological extract [2, 5]. The core nanoparticle synthesis involved the drop-by-step titration of this prepared extract into a dissolved metal precursor solution of a specific molarity. This mixture was subjected to continuous and vigorous magnetic stirring (e.g., at 600 rpm) at an optimized temperature (often around 70 °C) to facilitate the reaction [3, 5]. The active phytochemicals acted instantly to reduce the metal cations, a phase visually confirmed by a distinct color change in the suspension (e.g., transitioning from light to dark brown or black), indicating successful nucleation and precipitation [2, 4, 5]. To optimize the precipitation of metal hydroxides, the pH of the reaction mixture was frequently adjusted using precise volumes of NaOH or HCl solutions. Following the bio-reduction phase, the resulting solid precipitates were systematically collected via high-speed centrifugation and washed repeatedly with double-distilled water and absolute ethanol. This crucial step ensured the complete removal of unreacted precursor ions or residual organic biological matrix [13, 5]. The purified precipitates were then dried in a hot air oven at temperatures ranging from 60 °C to 100 °C. Finally, to eliminate any residual biological organic matter and achieve the desired highly crystalline metal oxide phase, a final calcination step in a muffle furnace was mandatory. The calcination temperatures were strictly controlled, predominantly set at 500 °C for a duration of 2 to 3 hours [2, 13, 8, 5].A comprehensive summary of these specific synthesis parameters extracted from the reviewed methodologies is systematically detailed in **Table II.3**.

Table II.3: Synthesis protocols and key operating conditions of the reviewed biogenic nanomaterials.

Synthesized Nanomaterials	*Plant Extract Source*	*Extract Ratio (Powder: Water)*	*Precursor Mixing Temp / Time*	*Drying Condition*	*Calcination Temperature / Time*	*Reference*
MgO@SnO_2@PVP NCs	*Pistacia lentiscus*	100 g : 1000 mL	75 °C / 3 h (Core) 50 °C / 2 h (Coating)	70 °C / 12 h	500 °C / 4 h	[2]
Ca/α-Fe_2O_3/ZnO/CuO NCs	*Mentha pulegium*	50 g : 500 mL	85 °C / 1 h	100 °C / 24 h	500 °C / 3 h	[13]
CS/Fe_3O_4 NCs	*Laurus nobilis & shrimp shells*	50 g : 500 mL	70 °C / 2 h (Core) 25 °C / 3 h (Coating)	60 °C / 24 h (Final)	500 °C / 4 h (Core only)	[3]
Ag@Fe_3O_4 NCs	*Laurus nobilis*	100 g : 1000 mL	70 °C / 4 h (Total)	70 °C / 12 h	400 °C / 4 h	[4]
ZnO@CuO NCs	*Mentha pulegium*	10 g : 100 mL	75 °C / 1 h	100 °C / 48 h	500 °C / 3 h	[8]
α-Fe_2O_3, CuO, ZnO NPs	*Portulaca oleracea*	250 g : 900 mL	70 °C / 2 h	100 °C / 48 h	500 °C / 3 h	[5]

While the specific operating parameters vary depending on the targeted metal oxides as detailed above, the physical laboratory procedure of green synthesis generally follows a universal step by step protocol. To better visualize this chronological sequence from the initial preparation of the plant extract and metal precursor mixing, to the final washing and calcination of the nanoparticles

a comprehensive schematic flowchart is illustrated in **Figure II.3**.

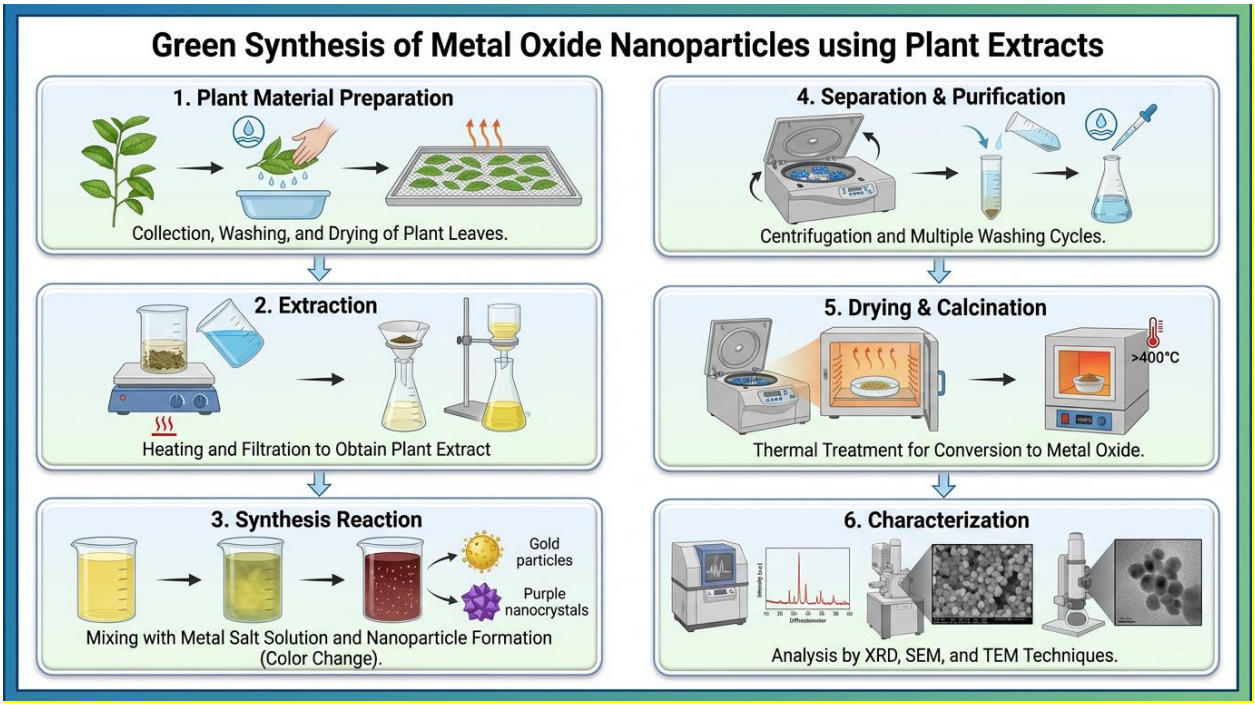

Figure II.3*:* Schematic representation of the plant-mediated green synthesis of metal oxide nanoparticles.

II.2.3 Preparation of Nanocomposites

To overcome the inherent limitations of pristine single metal oxides and significantly enhance their catalytic, magnetic, and adsorption performances, several reviewed studies advanced toward the fabrication of functionalized nanocomposites. These complex architectures strategically integrate distinct materials to generate powerful synergistic effects and maximize pollutant interaction. To significantly improve colloidal stability, active surface area, and biocompatibility, specific surface engineering and coating protocols were systematically applied. For instance, in the synthesis of the CS/Fe_3O_4 nanocomposite, biogenic iron oxide core nanoparticles were dispersed in an acidic solution and encapsulated within a dense, amine-rich chitosan polymeric shell via controlled co-precipitation. This modification successfully reversed the surface charge, maximizing the biological affinity and electrostatic attraction toward heavy metals [3]. Similarly, the structural modification of the MgO@SnO_2 system involved the integration of polyvinylpyrrolidone (PVP). This polymer acted as a robust steric stabilizer that effectively wrapped around the nucleating nanoparticles, preventing unwanted agglomeration during the synthesis phase and preserving a

uniformly high active surface area [2]. Beyond polymeric modifications, multimetallic oxides and metal-doped structures were successfully synthesized to boost distinct physicochemical properties. For example, Fe_3O_4 nanoparticles were doped with silver to form the $Ag@Fe_3O_4$ nanocomposite, deliberately introducing surface plasmon resonance effects [4]. Furthermore, complex multimetallic systems, such as the binary ZnO@CuO [8] and the highly complex quaternary system $Ca/\alpha\text{-}Fe_2O_3/ZnO/CuO$ [13], were engineered to create advanced heterojunction interfaces. These specifically designed heterojunctions play a critical role in suppressing photo-induced electron-hole recombination, thereby exponentially increasing the overall photocatalytic degradation efficiency of the resulting nanocomposites[60]. The structural design and strategic preparation of these functionalized nanocomposites are schematically illustrated in **Figure II.4**.

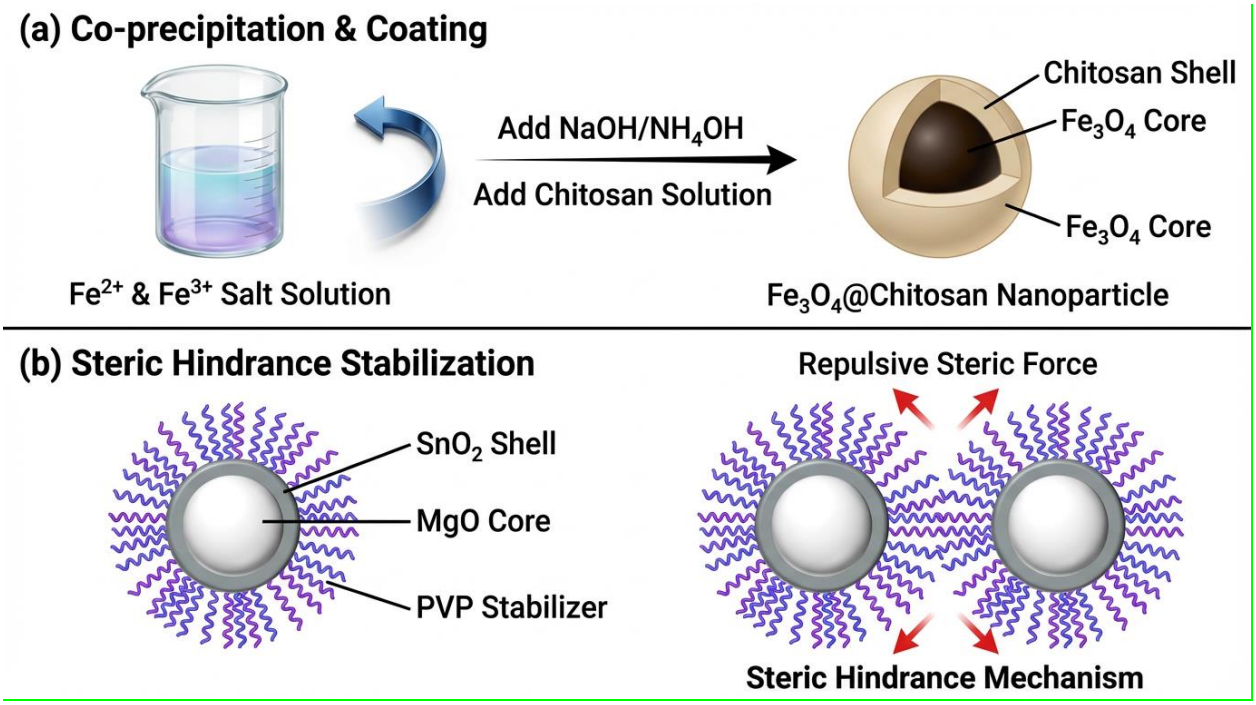

Figure II.4: Schematic representation of surface modification strategies for nanocomposites.

II.3 Characterization Techniques

To deeply understand the structural, morphological, optical, and functional properties of the green-synthesized nanomaterials, the reviewed studies employed a comprehensive suite of advanced analytical instruments.

II.3.1 X-Ray Diffraction (XRD)

XRD was utilized to rigorously determine the crystalline structure, phase purity, and average crystallite size[61]. The analyses were typically conducted using Cu Kα radiation (λ = 1.5406 Å) with operating voltages around 40 kV. The diffraction patterns were recorded over a 2θ scanning range from 10° to 80°. The Debye-Scherrer equation was universally applied to calculate the average crystallite size based on the most intense diffraction peaks [2, 13, 5]. Determining this precise crystallite size via XRD is crucial for validating the synthesis; a smaller nanoscale dimension drastically increases the surface-area-to-volume ratio[62]. This fundamental physical trait directly dictates the availability of unsaturated active sites, thereby significantly enhancing the maximum adsorption capacity for heavy metal cations[63].

Figure II.5: Benchtop X-ray diffractometer (XRD) apparatus used to determine the crystalline structure, phase purity, and crystallite size of the synthesized nanomaterials.

II.3.2 Scanning Electron Microscopy (SEM) and EDS

To investigate the surface topography and particle shape, SEM was extensively employed at accelerating voltages ranging from 15 to 20 kV. Furthermore, SEM was intrinsically coupled with Energy Dispersive Spectroscopy (EDS) to perform targeted elemental mapping, definitively confirming the chemical composition and elemental purity of the biosynthesized nanocomposites [13, 5]. Observing this specific morphology is vital, as it directly governs the diffusion kinetics of pollutants into the catalytic active sites[64]. Concurrently, the EDS analysis proves indispensable for validating the eco-friendly synthesis process by confirming the exact stoichiometric presence of the targeted metals while rigorously proving the absence of toxic chemical residues[65].

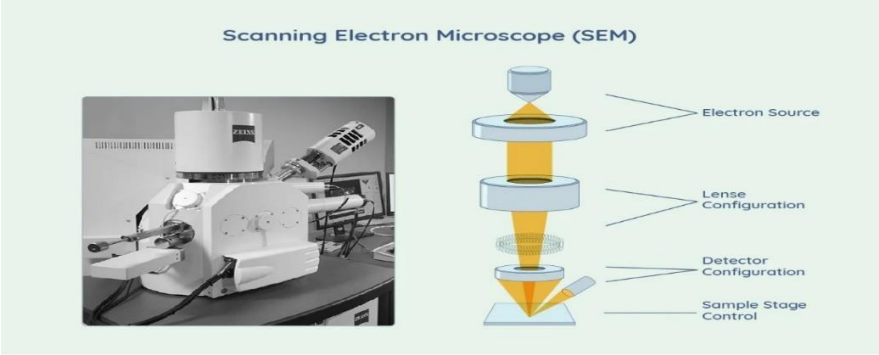

Figure II.6: Scanning Electron Microscope (SEM) instrument utilized for high-resolution morphological imaging and topographical analysis of the nanoparticles.

II.3.3 Fourier-Transform Infrared Spectroscopy (FTIR)

FTIR served as the primary tool to identify the functional groups originating from the plant extracts[66]. Using the KBr pellet technique, transmission spectra were recorded from 400 to 4000 cm^{-1}. This allowed for the precise detection of hydroxyl (-OH), carbonyl (C=O), and the characteristic low-frequency metal-oxygen (M-O) stretching vibrations [2, 3, 8]. Validating this biological capping layer via FTIR is essential because it not only proves the dual-role of the phytochemicals in preventing thermodynamic agglomeration, but also verifies the presence of the exact negatively charged functional groups required for the electrostatic binding of targeted pollutants[67].

Figure II.7: Fourier-Transform Infrared (FTIR) spectrometer employed for identifying surface functional groups and confirming the presence of plant-derived capping agents.

II.3.4 UV–Visible Spectroscopy and Zeta Potential

To evaluate the optical properties for photocatalytic applications, UV-Vis spectroscopy recorded absorbance across a 200 to 800 nm wavelength range to determine the optical energy band gap via the Tauc plot relation [4, 8]. Evaluating this optical band gap serves as a critical predictive tool for determining the photocatalytic performance; a narrower band gap confirms the material's ability to efficiently harvest low-energy visible solar light, making the macroscopic wastewater treatment process both highly scalable and energy-efficient[15]. Additionally, Zeta potential measurements quantified the surface charge and colloidal stability of the nanoparticles in aqueous environments, confirming the efficient steric capping provided by the phytochemicals and biopolymers [2, 3].

Figure II.8: UV-Visible spectrophotometer used for evaluating the optical absorbance properties and calculating the band gap energy of the nanocomposites.

A comprehensive summary of these characterization techniques and their primary applications is presented in **Table II.4**.

Table II.4: Summary of the advanced analytical techniques used for the characterization of the synthesized nanomaterials.

Primary Purpose / Information Obtained	*Abbreviation*	*Analytical Technique*
Determines crystalline structure, phase composition, and average crystallite size	**XRD**	X-ray Diffraction
Identifies surface functional groups and confirms the presence of plant-derived capping agents	**FTIR**	Fourier Transform Infrared Spectroscopy

Primary Purpose / Information Obtained	*Abbreviation*	*Analytical Technique*
Analyzes the surface morphology, shape, and approximate particle size of the nanomaterials	**SEM**	Scanning Electron Microscopy
Confirms the elemental composition and evaluates the chemical purity of the samples	**EDX**	Energy Dispersive X-ray Spectroscopy
Studies optical properties, determines light absorption, and calculates the band gap energy	**UV-Vis**	UV–Visible Spectroscopy
Evaluates the surface charge and stability of nanoparticles in aqueous suspensions	**-**	Zeta Potential Analysis

II.4 Pollutant Removal Experiments

The practical environmental applications of the synthesized nanocomposites were evaluated through systematically designed batch experimental setups, simulating real industrial wastewater treatment conditions.

II.4.1 Adsorption Experimental Setup

For heavy metal sequestration, experiments were conducted using temperature-controlled orbital shakers. Typically, a precise dosage of the nano adsorbent (ranging from 10 to 50 mg) was dispersed into Erlenmeyer flasks containing 50 to 100 mL of heavy metal solutions with initial concentrations varying from 10 to 100 mg/L. The mixtures were continuously agitated at speeds between 150 and 200 rpm to ensure maximum solid-liquid interfacial contact [2, 13, 3]. Critical operating parameters were systematically varied: the initial pH was adjusted using 0.1 M HCl or NaOH (investigated across a broad range of 2 to 10), and the contact time was precisely monitored up to 180 minutes until thermodynamic equilibrium was achieved. The sequential stages of the batch adsorption process are illustrated in **Figure II.9**.

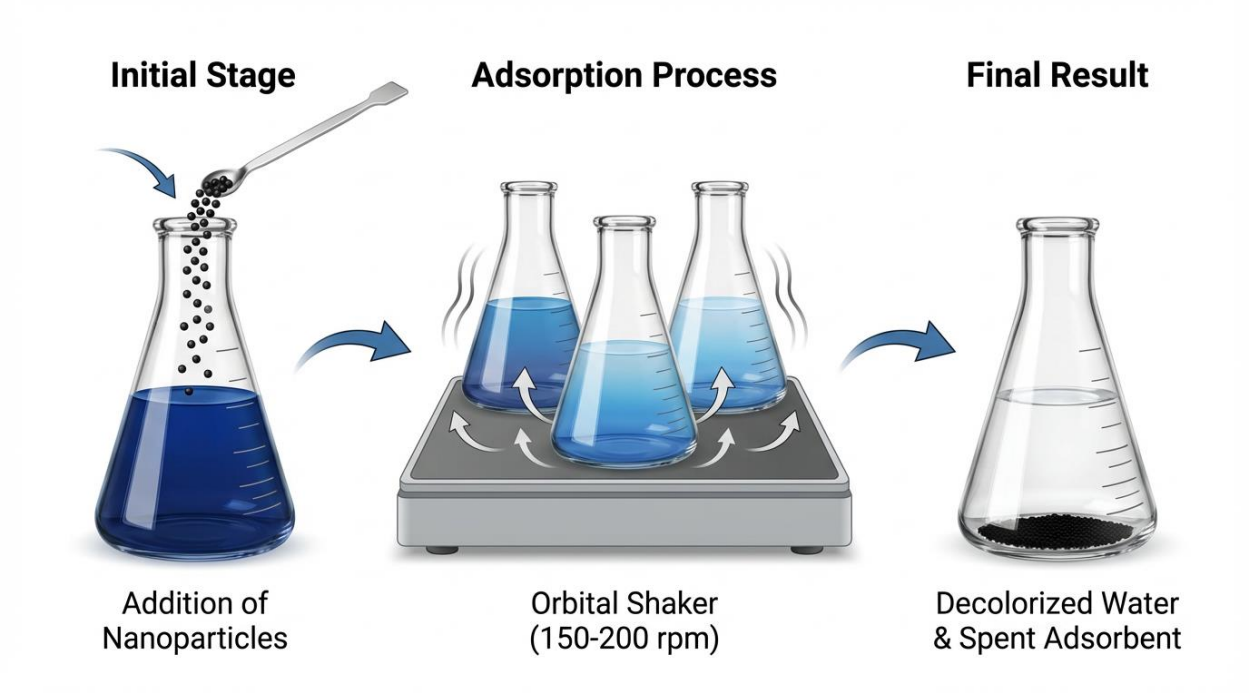

Figure II.9*:* Schematic diagram illustrating the batch adsorption experimental setup for pollutant removal using an orbital shaker.

II.4.2 Photocatalytic Degradation Setup

In studies addressing the degradation of organic pollutants and synthetic dyes [4, 8], the nano-photocatalysts were dispersed in the pollutant solutions and initially stirred in absolute darkness for 30 to 60 minutes to establish an adsorption-desorption equilibrium. Subsequently, the suspension was exposed to targeted light sources (such as visible light or 300 W Xenon lamps) positioned at a fixed distance from the reactor. Aliquots were extracted at regular time intervals, centrifuged, and analyzed to track the degradation kinetics.

II.4.3 Real Oil and Hydrocarbon Remediation Procedures

For the treatment of real petroleum wastewater [2, 8, 5], the green nanocomposites were directly dosed into the raw oily wastewater samples under vigorous mechanical stirring. The treatment efficiency was quantitatively determined by measuring the drastic reduction in chemical oxygen demand (COD), total suspended solids (TSS), and the residual oil-in-water concentration after specific contact periods.

II.4.4 Pollutant Removal and Degradation Efficiency

The overall treatment performance, expressed as the removal efficiency (R%) for heavy metals and suspended solids, or the photocatalytic degradation efficiency ($D\%$) for organic dyes and hydrocarbons, was systematically calculated using the relative difference between the initial and final pollutant concentrations. The standard equation employed is:

$$Removal\ \ Efficiency\ (\%) = \frac{c_0 - c_t}{c_0} \times\ 100$$

Where:

- c_0 **(mg/L):** represents the initial baseline concentration of the targeted pollutant in the aqueous solution (or raw wastewater) prior to the introduction of the nanomaterials.
- c_t **(mg/L):** is the residual concentration of the pollutant at any specific contact time (t), or at thermodynamic equilibrium (c_e).
- In the context of organic dyes and spectrophotometric analyses [3, 4], the concentration terms in the equation were directly substituted by their corresponding maximum optical absorbance values (A^0 for initial absorbance and At for absorbance at time t) derived from UV-Vis spectroscopy.

II.4.5 Adsorption Capacity Calculations

To determine the exact mass of the pollutant sequestered per unit mass of the green nanoadsorbent, mass balance equations were strictly utilized. The equilibrium adsorption capacity (qe ,expressed in mg/g), expressed in mg/g) and the time-dependent adsorption capacity (qt mg/g) are fundamental parameters for evaluating the economic feasibility and maximum saturation point of the synthesized materials. The governing equations are as follows:

$$q_e = \frac{(C_0 - C_e) \times V}{m}$$

$$q_t = \frac{(C_0 - C_t) \times V}{m}$$

Where:

- $\boldsymbol{q_e}$ and $\boldsymbol{q_t}$ **(mg/g):** denote the amount of heavy metal ions or organic pollutants adsorbed onto the surface of one gram of the nanomaterial at equilibrium and at a predetermined time (t), respectively.

- V **(L):** is the total volume of the simulated pollutant solution or the real petroleum wastewater sample used in the batch experiment.
- m **(g):** is the precise dry mass (dosage) of the green-synthesized nanocomposite introduced into the reaction system.
- C_e **(mg/L):** represents the pollutant concentration in the liquid phase once the adsorption-desorption thermodynamic equilibrium has been fully established.

These standardized mathematical models provided the foundational data required by the reviewed studies to further plot and investigate complex adsorption isotherms (Langmuir and Freundlich) and kinetic models (pseudo-first-order and pseudo-second-order) in their respective discussions[2,8].

II.5 Reusability of photocatalytic degradation

After completing the adsorption or photocatalytic treatment, the spent nanocomposites were separated from the aqueous phase. For magnetic materials like the biogenic Fe_3O_4 cores [3, 4], separation was achieved using an external neodymium magnet, which avoided the need for centrifugation. For non-magnetic nanoparticles, standard centrifugation was used to collect the solid mass. Following recovery, the loaded adsorbents underwent chemical desorption to release the bound pollutants. To desorb heavy metal cations, the materials were typically treated with dilute acid (0.1 M HCl or 0.1 M HNO_3) under continuous agitation for 60 to 120 minutes. The high proton (H^+) concentration in these solutions competed with the metal ions for surface active sites, disrupting the coordinate bonds and releasing the metals into the solution. When dealing with organic pollutants, absolute ethanol was commonly used as the desorbing agent to extract the trapped hydrophobic molecules. Following desorption, the regenerated nanomaterials required washing to remove any remaining acid. They were rinsed repeatedly with double-distilled water until the washing solution reached a neutral pH. The washed nanoparticles were then transferred to glass Petri dishes and dried in an oven at 60 °C to 80 °C for several hours. This step ensured the removal of moisture without degrading the capping biopolymers. The dried nanocomposites were subsequently weighed and introduced into fresh pollutant solutions for the next treatment cycle. This regeneration process was repeated for up to five consecutive cycles across the reviewed

studies to evaluate the reusability of the green-synthesized materials. Tracking the performance over multiple cycles allowed researchers to measure the gradual decline in adsorption capacity and verify the structural stability of the nanomaterials for potential industrial applications [2, 3, 8, 5]. The complete cyclic regeneration process is illustrated in **Figure II.10**.

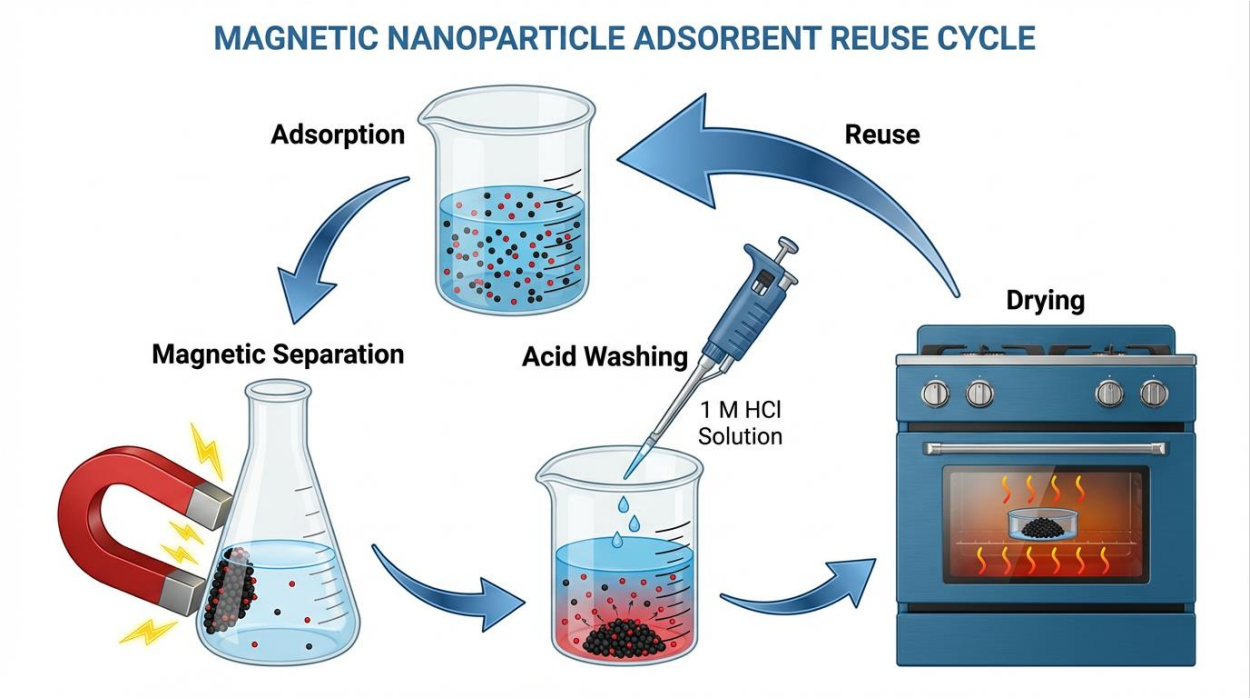

Figure II.10: Schematic of the cyclic regeneration and recovery process for magnetic nanocomposites.

Chapter III. Performance Analysis and Characterization of the Reviewed Nanomaterials

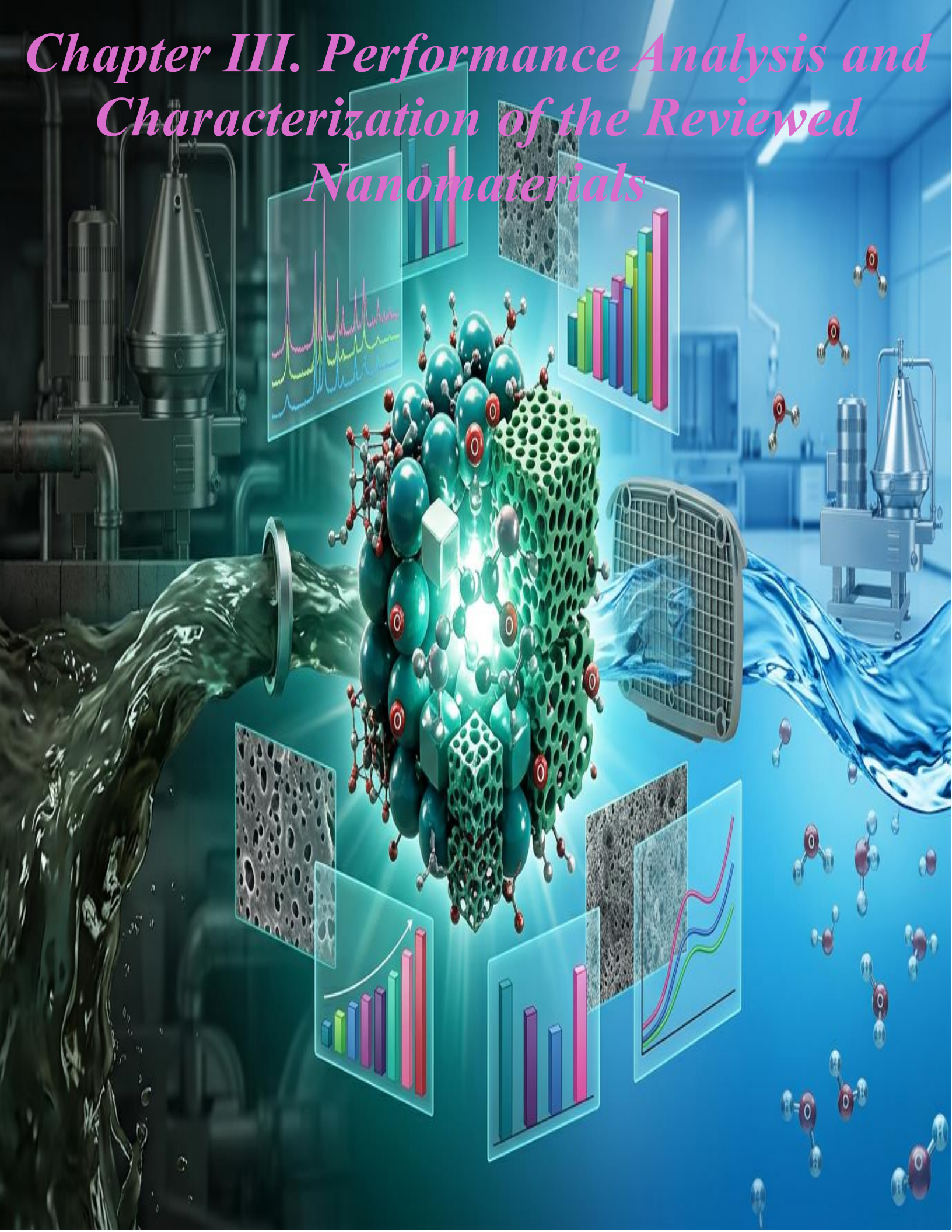

III. Introduction

This chapter presents and comprehensively discusses the main findings reported in the reviewed studies regarding the synthesis, characterization, and environmental applications of green-synthesized metal oxide nanomaterials for wastewater treatment. The discussion highlights the specific data, kinetic models, and comparative efficiencies of the different nanocomposites.

III.1 Structural and Morphological Characterization of Nanomaterials

The reviewed studies successfully confirmed the fabrication of highly pure metal oxide nanoparticles and nanocomposites using plant-mediated green synthesis methods. The structural and morphological integrity of these materials was validated through a series of advanced analytical techniques.

III.1.1 Crystallographic Analysis (XRD)

Structural analysis using X-ray Diffraction (XRD) consistently demonstrated the formation of highly crystalline phases corresponding to specific targeted metal oxides (such as ZnO, Fe_2O_3, CuO, MgO, and SnO_2). The diffraction peaks perfectly matched standard reference patterns, confirming the high purity of the synthesized structures without secondary phase impurities. The specific average crystallite sizes were precisely calculated using the Debye-Scherrer equation. For instance, the calculations yielded precise nanoscale dimensions of 20.12 nm for hematite (α-Fe_2O_3), 22.25 nm for CuO, and 25.04 nm for ZnO nanoparticles [5]. Across the complex binary and quaternary nanocomposites, the crystallite sizes generally ranged between 30 and 80 nm, confirming the successful confinement of the materials at the nanoscale. These structural confirmations are comprehensively illustrated in the comparative XRD patterns shown in **Figure III.1**

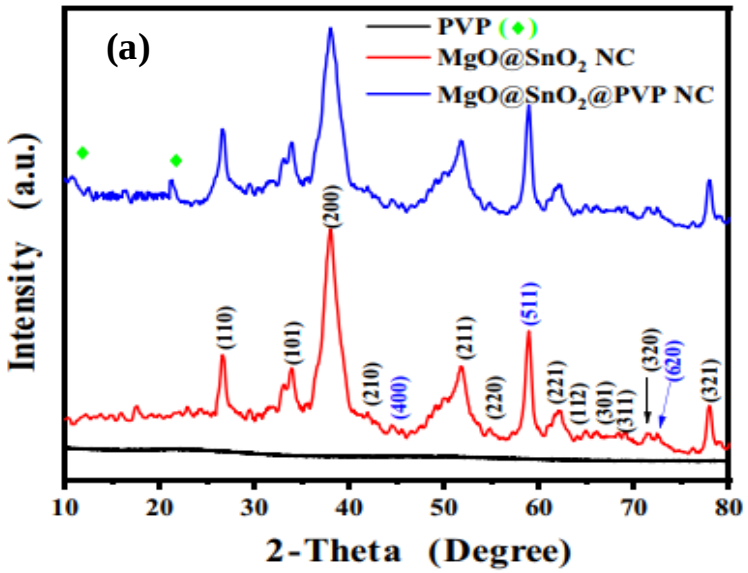
(a)
PVP (♦)
MgO@SnO2 NC
MgO@SnO2@PVP NC
Intensity (a.u.)
(110)
(101)
(200)
(210)
(400)
(211)
(220)
(511)
(221)
(112)
(301)
(311)
(320)
(620)
(321)
10 20 30 40 50 60 70 80
2-Theta (Degree)

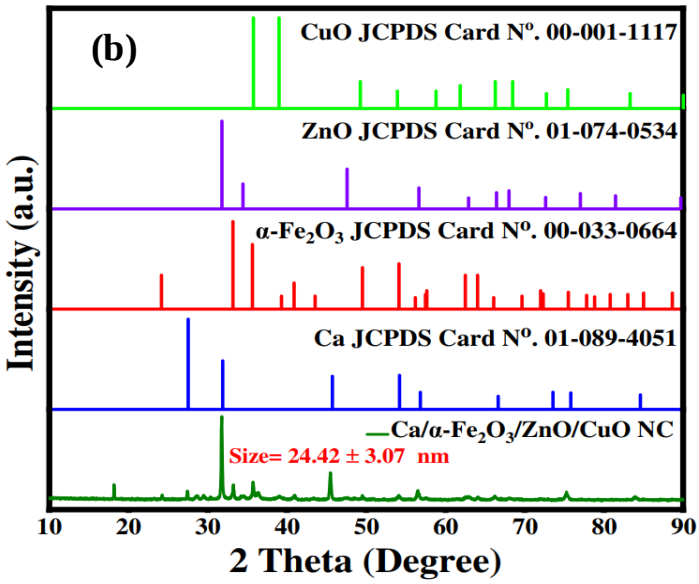
(b)
CuO JCPDS Card N°. 00-001-1117
ZnO JCPDS Card N°. 01-074-0534
α-Fe2O3 JCPDS Card N°. 00-033-0664
Ca JCPDS Card N°. 01-089-4051
Ca/α-Fe2O3/ZnO/CuO NC
Size= 24.42 ± 3.07 nm
Intensity (a.u.)
10 20 30 40 50 60 70 80 90
2 Theta (Degree)

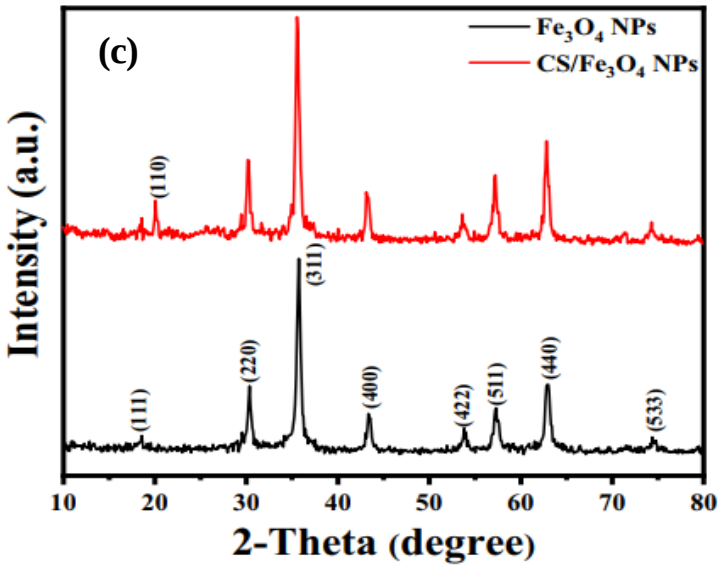
(c)
Fe3O4 NPs
CS/Fe3O4 NPs
Intensity (a.u.)
(110)
(111)
(220)
(311)
(400)
(422)
(511)
(440)
(533)
10 20 30 40 50 60 70 80
2-Theta (degree)

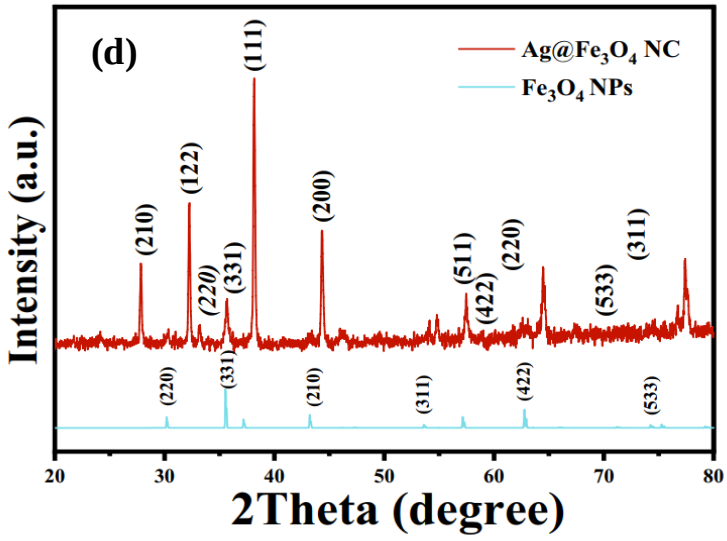
(d)
Ag@Fe3O4 NC
Fe3O4 NPs
Intensity (a.u.)
(210)
(122)
(220)
(331)
(111)
(200)
(511)
(422)
(220)
(533)
(311)
20 30 40 50 60 70 80
2Theta (degree)

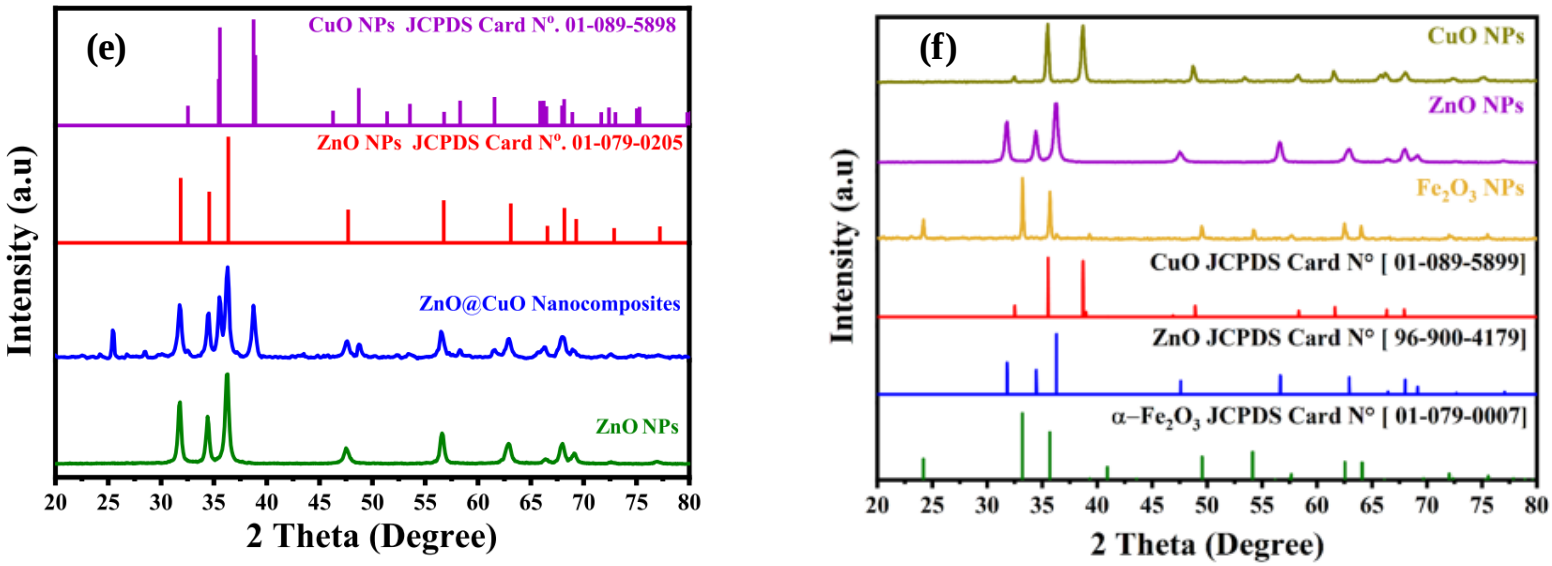

Figure III.1: Comprehensive comparative X-ray Diffraction (XRD) patterns confirming the crystalline phases of all green-synthesized nanomaterials[2,5,4,3,13,2].

III.1.2 Morphological and Elemental Profiling (SEM & EDX)

Morphological analysis via Scanning Electron Microscopy (SEM) revealed that the synthesized nanoparticles exhibited distinct nanoscale features, predominantly forming spherical, near-spherical, or mildly aggregated structures [2, 13, 5]. This confirmed nanoscale dimension significantly increases the specific surface area, providing abundant active sites essential for heavy metal adsorption and catalytic reactions. Furthermore, Energy Dispersive X-ray Spectroscopy (EDX) analysis definitively confirmed the elemental composition of the synthesized nanomaterials. The respective EDX spectra demonstrated the exclusive presence of the expected parent metal and oxygen elements, effectively ruling out any significant chemical impurities and validating the cleanliness of the green synthesis route. These distinct morphological variations and highly porous surface structures are clearly depicted in the comparative SEM micrographs in **Figure III.2**.

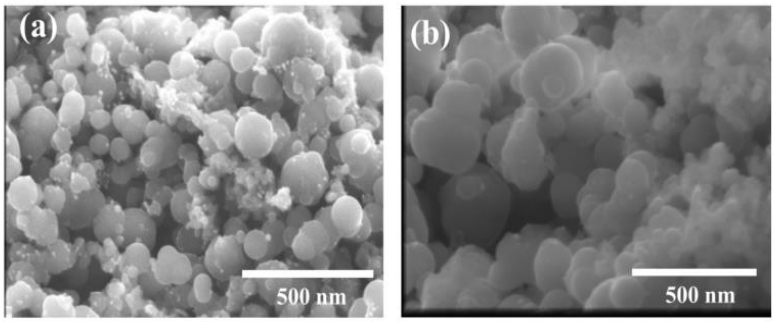

(a)

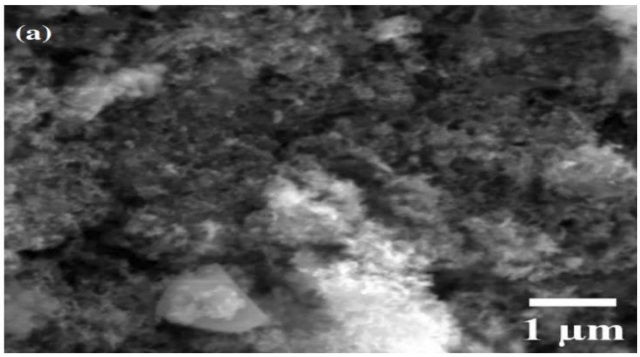

(b)

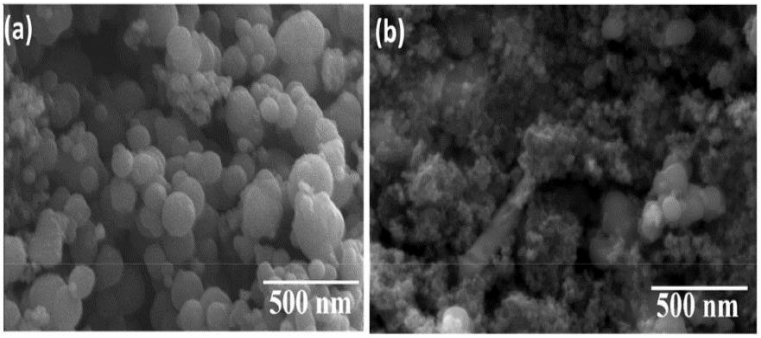

(c)

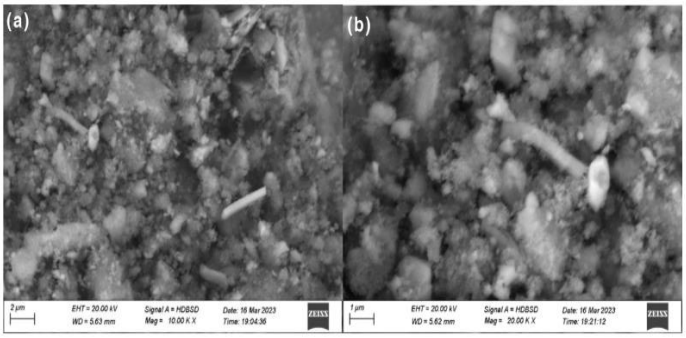

(d)

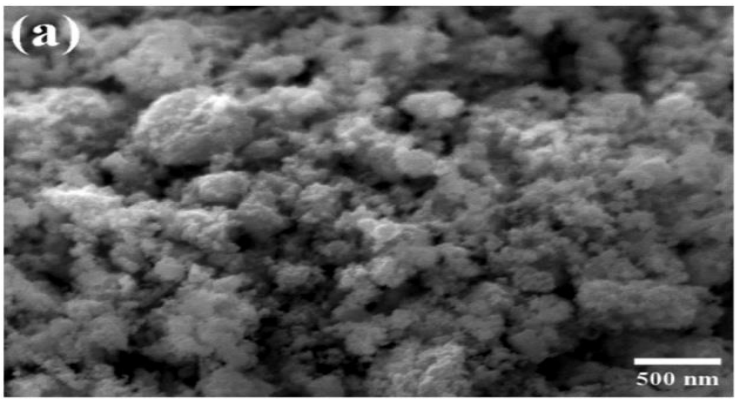

(e)

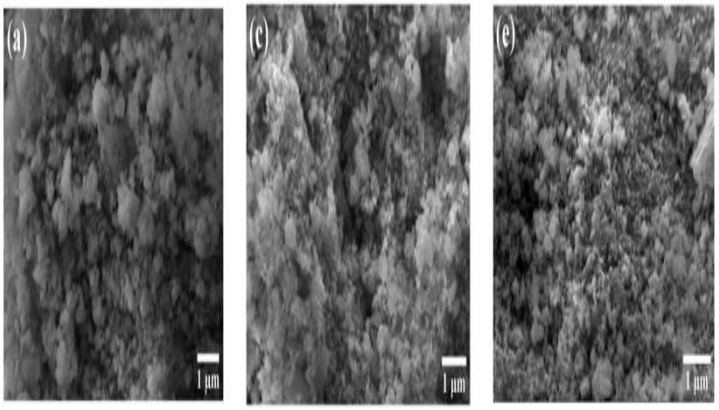

(f)

Figure III.*2*: Scanning Electron Microscopy (SEM) images illustrating the diverse morphological features of the green-synthesized nanomaterials[2,5,4,3,13,2].

III.1.3 Functional Group Identification (FTIR)

To understand the dual role of the plant extracts as both reducing and capping agents, Fourier-Transform Infrared Spectroscopy (FTIR) results were critically evaluated. The FTIR spectra across the studies consistently exhibited distinct absorption bands corresponding to hydroxyl (-OH),

carbonyl (C=O), and amine (-NH) stretching vibrations. These organic functional groups unequivocally originated from the phytochemicals (such as polyphenols and flavonoids) present in the leaf extracts (*Portulaca oleracea*, *Mentha pulegium*, etc.), confirming their successful binding to the nanoparticles' surfaces. Additionally, characteristic low-frequency bands (typically below 600 cm^{-1}) were observed, representing the specific metal-oxygen (M-O) stretching vibrations, thereby confirming the formation of the metal oxide cores [2, 3, 8]. These characteristic functional groups and specific metal-oxygen molecular vibrations are comprehensively validated in the comparative FTIR spectra presented in **Figure III.3.**

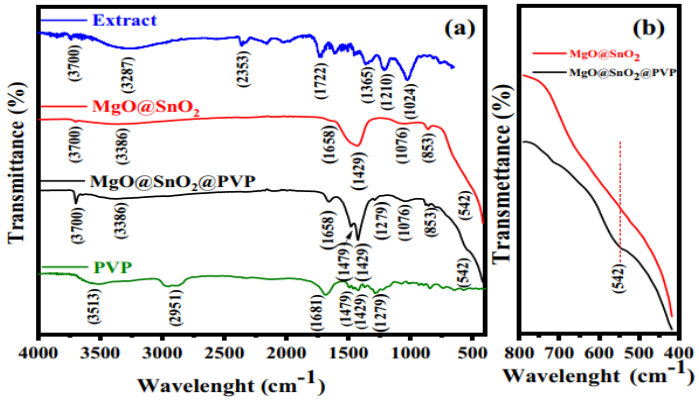

(a)

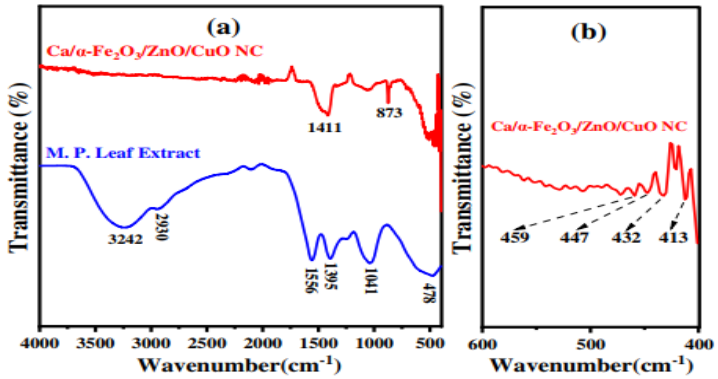

(b)

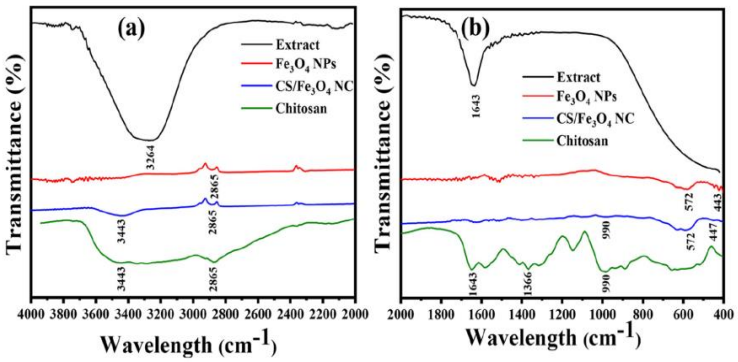

(c)

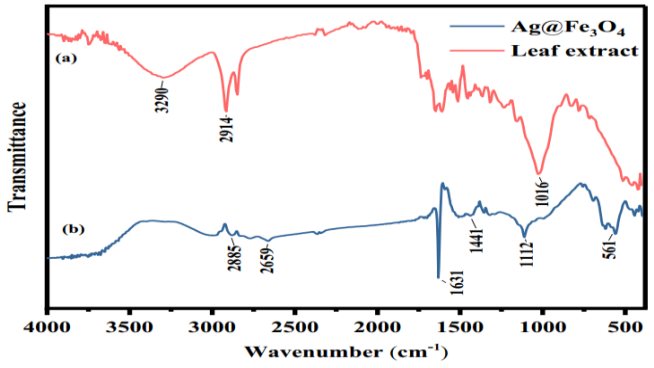

(d)

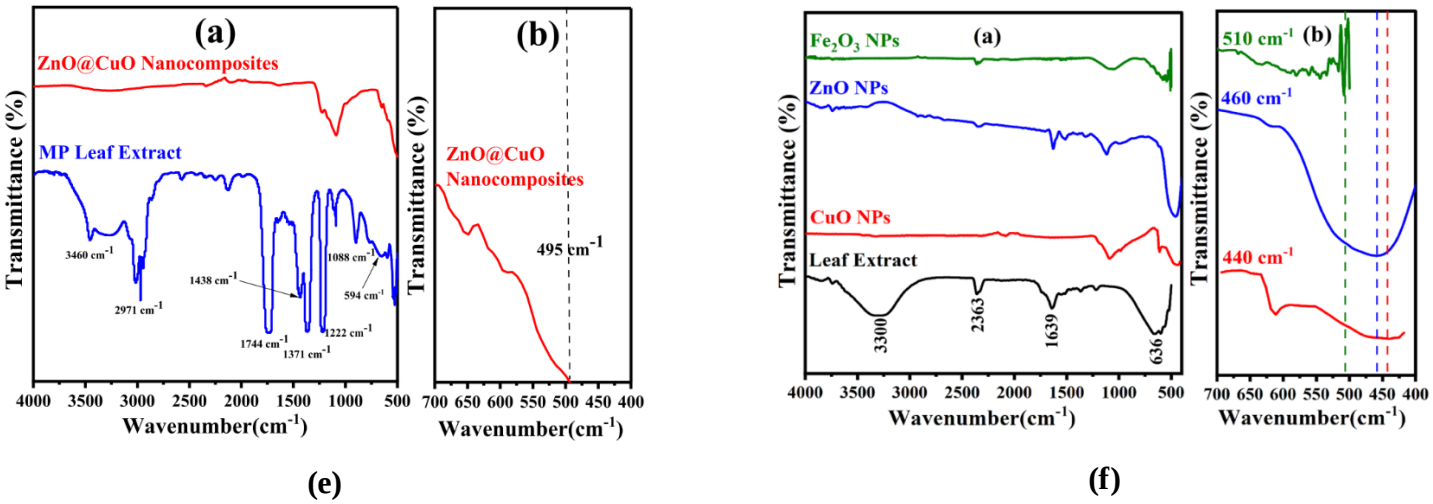

Figure III.3 : Comparative Fourier-Transform Infrared (FTIR) spectra confirming the functional groups of the plant extracts and the successful formation of metal-oxygen bonds in the green-synthesized nanomaterials[2,5,4,3,13,2].

III.2 Optical and Surface Properties of the Nanomaterials

The interaction of the synthesized nanomaterials with light and their stability in aqueous environments are critical parameters that directly dictate their performance in photocatalysis and adsorption, respectively[68].

III.2.1 Optical Band Gap Analysis (UV-Vis)

Optical characterization using UV-Visible spectroscopy was systematically performed to determine the light absorption capacity and to calculate the optical energy band gap (Eg) of the metal oxide semiconductors via Tauc plots. The reviewed studies reported a diverse range of band gap energies highly dependent on the complexity of the nanocomposite. For highly complex heterojunctions, the band gap was successfully narrowed. Specifically, the reported band gap energies ranged from a highly active 1.98 eV for the organically modified MgO@SnO_2@PVP nanocomposite [2] to 3.07 eV for the multimetallic Ca/α-Fe_2O_3/ZnO/CuO system [13]. This deliberate narrowing of the band gap fundamentally enhanced the capacity of the nanocomposites to absorb visible light, thereby preventing the fast recombination of electron-hole pairs and significantly boosting continuous photocatalytic degradation efficiency[15]. a comprehensive comparison of the calculated band gap energies is illustrated in **Figure III.4**.

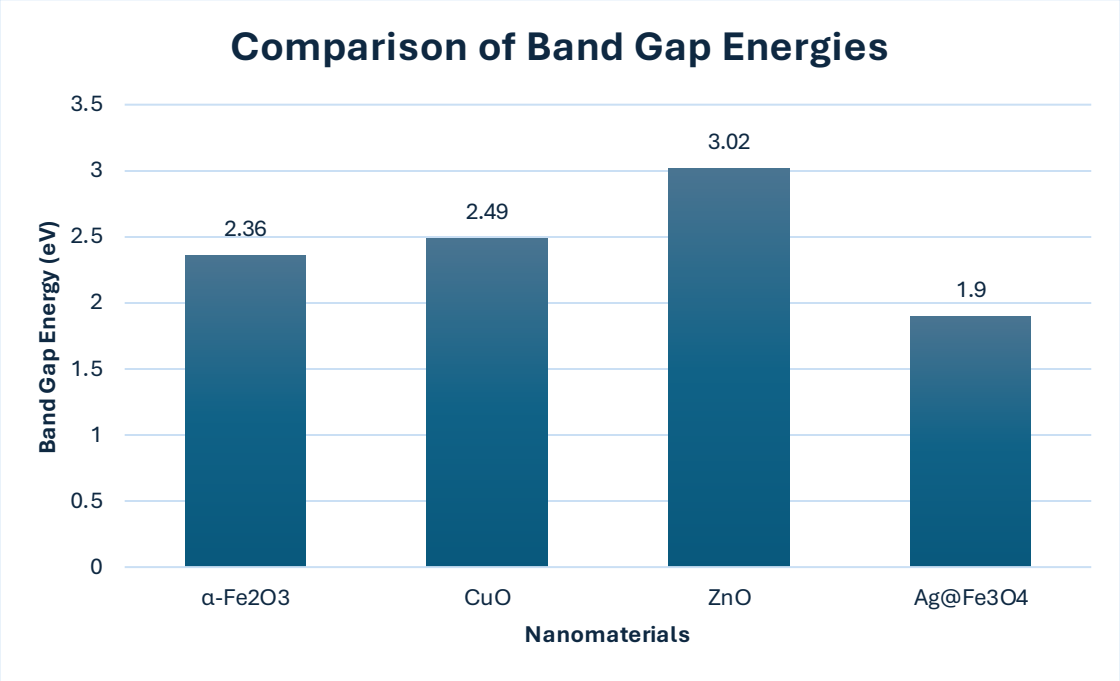

Figure III.4: Comparison of the calculated band gap energies for the synthesized single metal oxides and the multimetallic nanocomposite.

III.2.2 Surface Charge and Colloidal Stability (Zeta Potential)

The colloidal stability and the nature of the surface electrostatic interactions were quantitatively assessed through Zeta potential measurements. The absolute values of the Zeta potential were found to be highly indicative of the nanomaterials' dispersion stability. For instance, unmodified biogenic nanoparticles exhibited strong negative surface charges, such as -27.6 mV for the ZnO@CuO nanocomposite [8] and -33.6 mV for bare Fe_3O_4 nanoparticles [3], indicating excellent stability due to strong electrostatic repulsion provided by the plant capping agents. Interestingly, surface modification protocols completely altered this dynamic; the polymer coating in the CS/Fe_3O_4 nanocomposite shifted the Zeta potential to a distinct positive value of +18.9 mV [3]. This specific positive surface charge critically maximized the biological and electrostatic affinity of the nanocomposite towards negatively charged or highly polarized heavy metal species in the subsequent wastewater treatment experiments.

III.3 Removal of Heavy Metals from Wastewater

The practical environmental remediation performance of the synthesized green nanomaterials was rigorously evaluated across the reviewed studies. The experimental data conclusively demonstrated

that these materials possess exceptional adsorption capacities for a diverse array of wastewater pollutants.

III.3.1 Heavy Metal Sequestration Efficiency

The removal of highly toxic heavy metal ions (such as Pb^{2+}, Cd^{2+}, Cr^{6+}, Ni^{2+}, and As^{3+}) from real petroleum wastewater and contaminated sludge yielded consistently outstanding results. Across the studies, removal efficiencies ranged from 84.1% in highly complex sludge matrices [13]to an absolute 100% in aqueous solutions [3, 8, 5]. The highest overall performance was distinctly achieved by the multimetallic nanocomposites. For instance, both the $Ag@Fe_3O_4$ nanocomposite [4] and the ZnO@CuO heterojunction [8] achieved near-complete eradication (99% to 100%) of all targeted heavy metals within an exceptionally short contact time of just 30 minutes. This rapid uptake is attributed to the synergistic effect of the expanded specific surface area and the abundance of oxygen-containing functional groups provided by the plant extracts. The maximum removal efficiencies achieved by the various nanocomposites are summarized in **Figure III.5**.

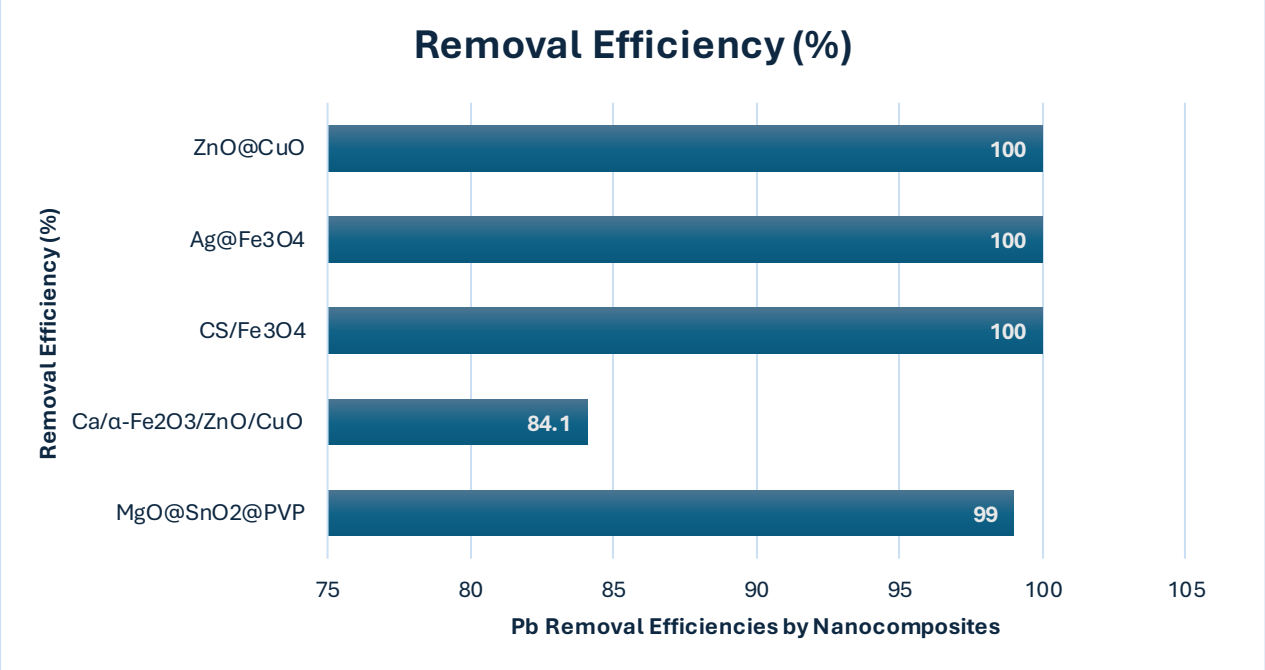

Figure III.5: Maximum heavy metal removal efficiencies achieved by the green-synthesized nanocomposites under optimized conditions.

III.4 Removal of Hydrocarbons and Oil Contaminants

Petroleum wastewater contains complex mixtures of hydrocarbons and oil-in-water (OIW) emulsions that are highly resistant to conventional treatments. The reviewed studies systematically evaluated the efficiency of various green-synthesized nanomaterials in reducing Total Petroleum Hydrocarbons (TPH), OIW content, and Total Suspended Solids (TSS). While unmodified single metal oxide nanoparticles and certain synthesized structures demonstrated moderate to high capabilities, achieving approximately 80% removal for OIW and 70% for TSS [5], engineered nanocomposites exhibited vastly superior performance. For instance, the comprehensive analysis of the chitosan-coated CS/Fe_3O_4 nanocomposite revealed exceptional capabilities, improving the OIW removal rate to 90% and showing distinct time-dependent efficiency curves [3]. Furthermore, comparative kinetic and efficiency studies explicitly demonstrated that the functionalized nanocomposites significantly outperform bare magnetic nanoparticles under identical experimental conditions. More remarkably, the plasmonic Ag@Fe_3O_4 nanocomposite achieved an unprecedented 98% removal of TPH and 91.8% removal of TSS [4]. This significant enhancement in hydrocarbon degradation and oil separation is directly attributed to the surface modifications, the high surface area of the nanostructures, and their robust catalytic activity that promotes the breakdown of complex hydrocarbon chains. The comprehensive removal efficiencies and the comparative performance of these diverse nanomaterials are visually detailed in **Figure III.6**.

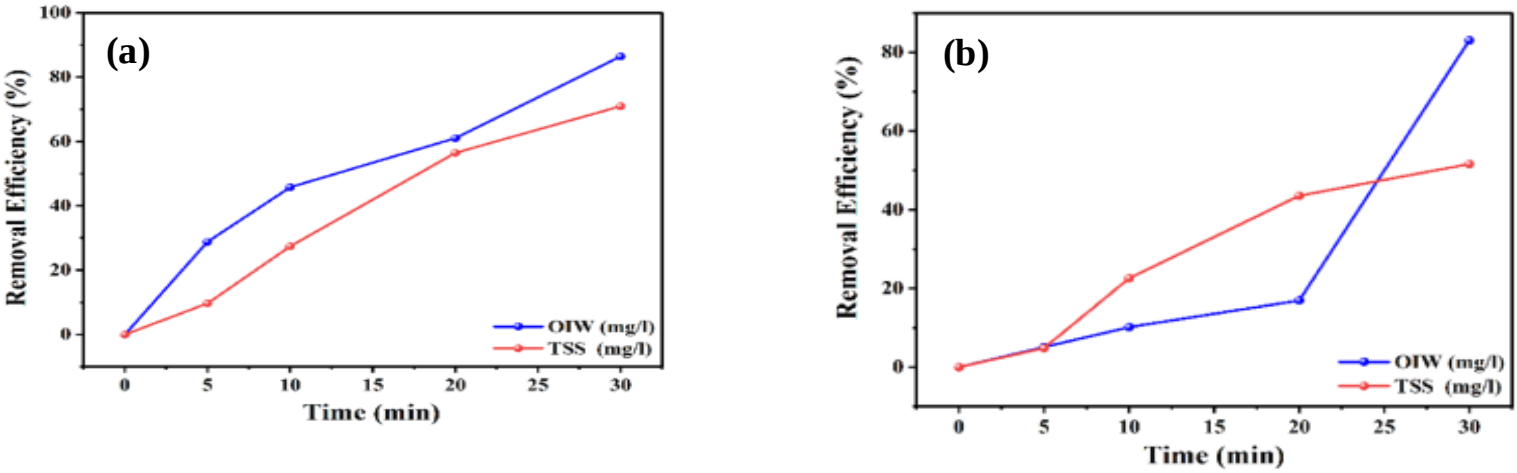

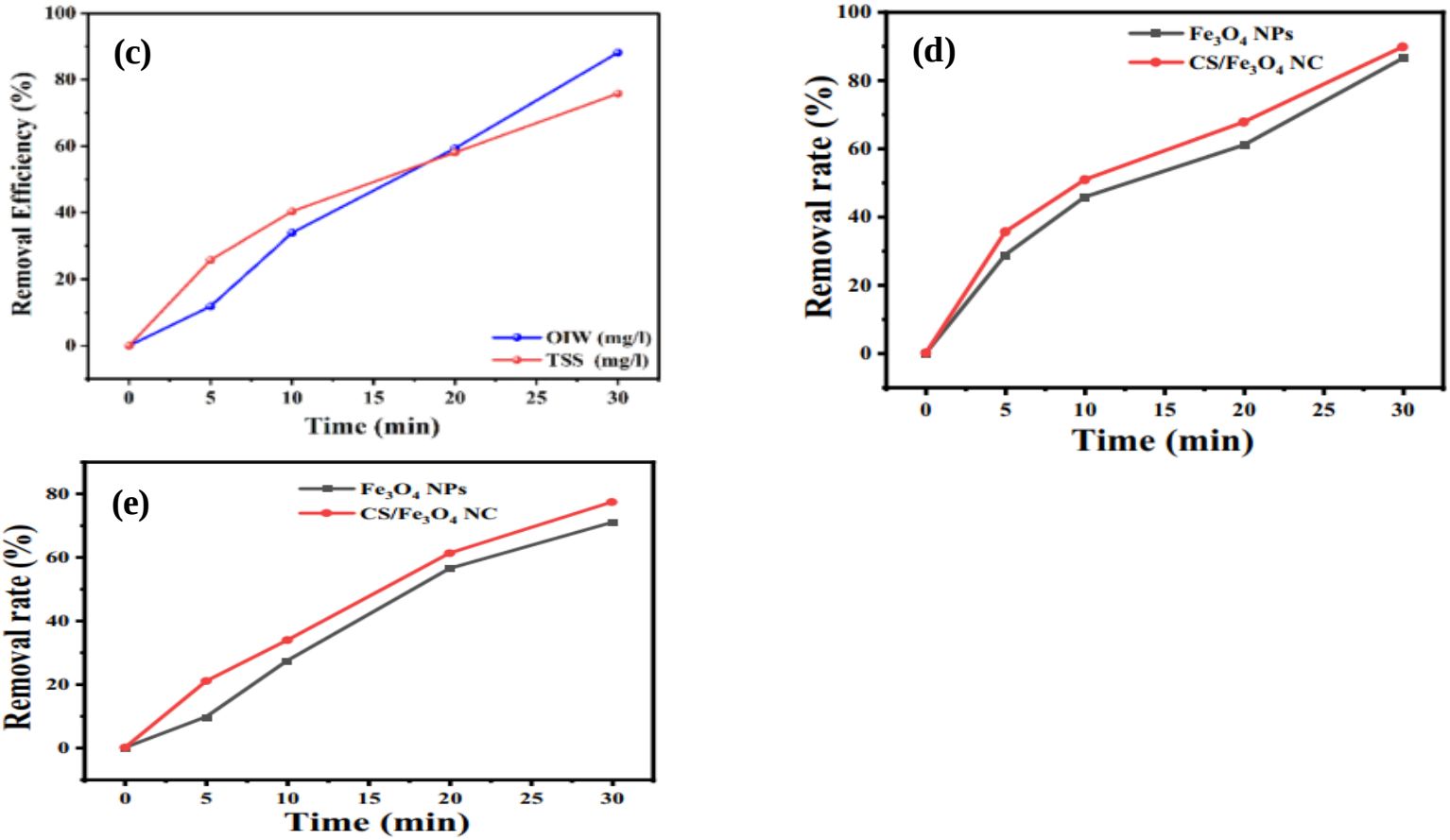

Figure III.6: Comparative evaluation of hydrocarbon, OIW, and TSS removal efficiencies using various green-synthesized nanomaterials[2,5,4,3,13,2].

III.5 Photocatalytic Degradation of Organic Pollutants

Synthetic organic dyes, such as Methylene Blue (MB) and Rhodamine B (RB), represent a major environmental challenge due to their complex, highly stable aromatic structures that resist conventional biological degradation[69]. The reviewed studies emphasize the exceptional capability of green-synthesized nanomaterials in the photocatalytic degradation of these persistent organic pollutants under light irradiation. The integration of specific nanoparticles into complex heterojunctions significantly restricts the rapid recombination of photo-induced electron-hole pairs, thereby enhancing the generation of reactive oxygen species (ROS)[70]. For instance, the chitosan-coated CS/Fe_3O_4 nanocomposite demonstrated remarkable catalytic properties, achieving a 99% degradation efficiency for Methylene Blue (MB) within just 75 minutes of exposure, as evidenced by the rapid decline in its kinetic curves [3]. Furthermore, the synthesis of the plasmonic $Ag@Fe_3O_4$ nanocomposite proved highly effective for even more complex molecules, successfully

degrading 96.8% of Rhodamine B (RB) [4]. Beyond their initial degradation efficiency, both functionalized nanocomposites exhibited remarkable structural stability, maintaining exceptionally high removal rates (above 94%) even after five consecutive reuse cycles. This confirms their economic viability for large-scale applications. The comprehensive degradation kinetics (C_t/C_0vs time) and the robust reusability profiles of these specific nanocomposites against organic dyes are visually detailed in **Figure III.7**.

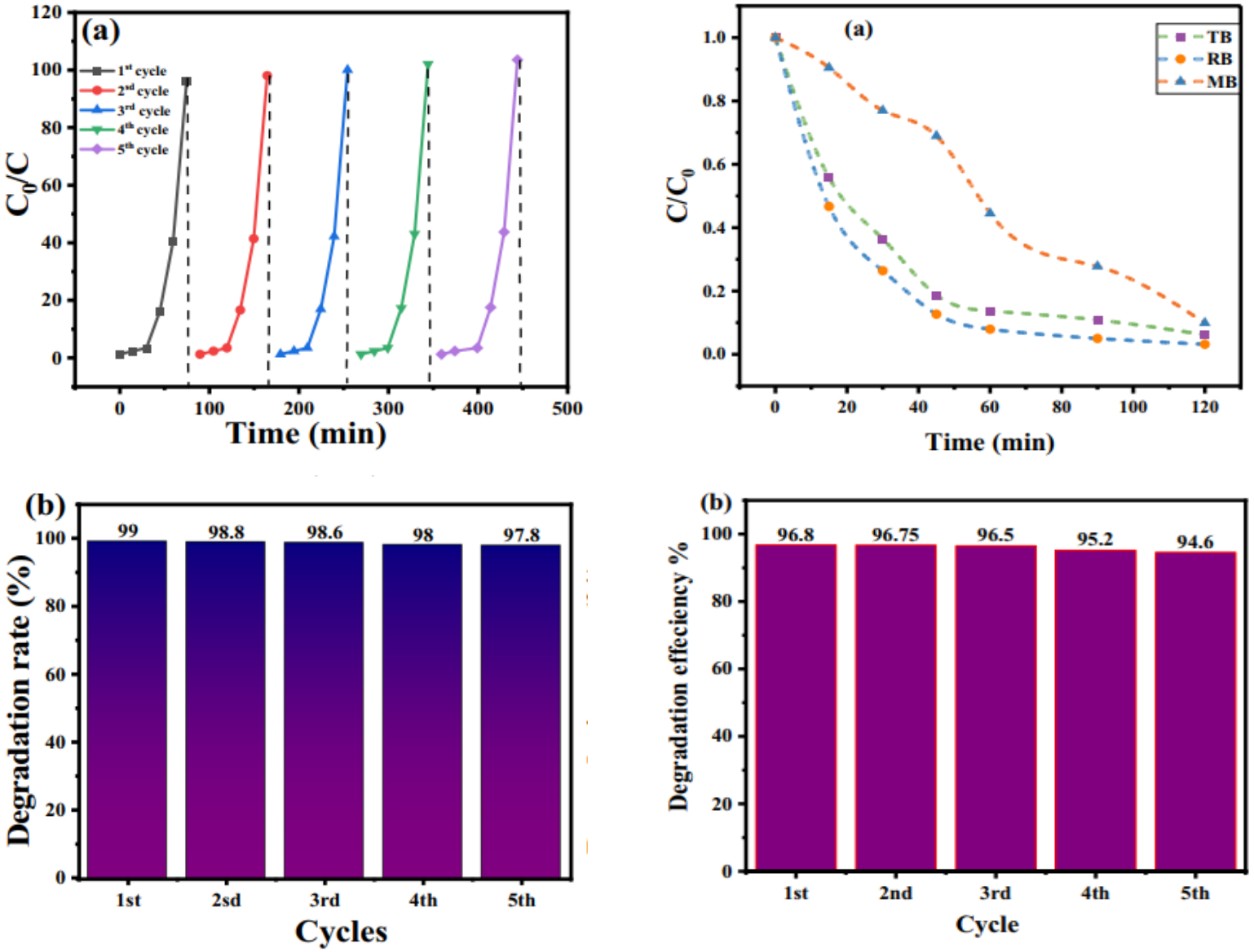

Figure III.7: Comprehensive photocatalytic degradation performance of organic dyes[3,4].

III.6 Comparison Between Different Nanocomposites

A comprehensive evaluation of the reviewed studies establishes that engineering bare metal oxide nanoparticles into binary, ternary, or functionalized nanocomposites dramatically enhances their environmental remediation capabilities. While single-metal oxides, such as isolated ZnO, CuO, and α-Fe_2O_3, demonstrate baseline removal efficiencies for suspended solids and specific heavy metals [5], their large-scale application is frequently limited by rapid electron-hole recombination rates and a high tendency for nanoparticle agglomeration[71]. In stark contrast, the development of complex heterojunctions and coated nanocomposites systematically overcomes these intrinsic limitations through strategic synergistic interactions[15]. For instance, coupling different bandgap materials, such as in the binary ZnO@CuO system, creates an effective charge separation interface that significantly extends the lifetime of reactive oxygen species, thereby pushing removal efficiencies to optimal levels [8].

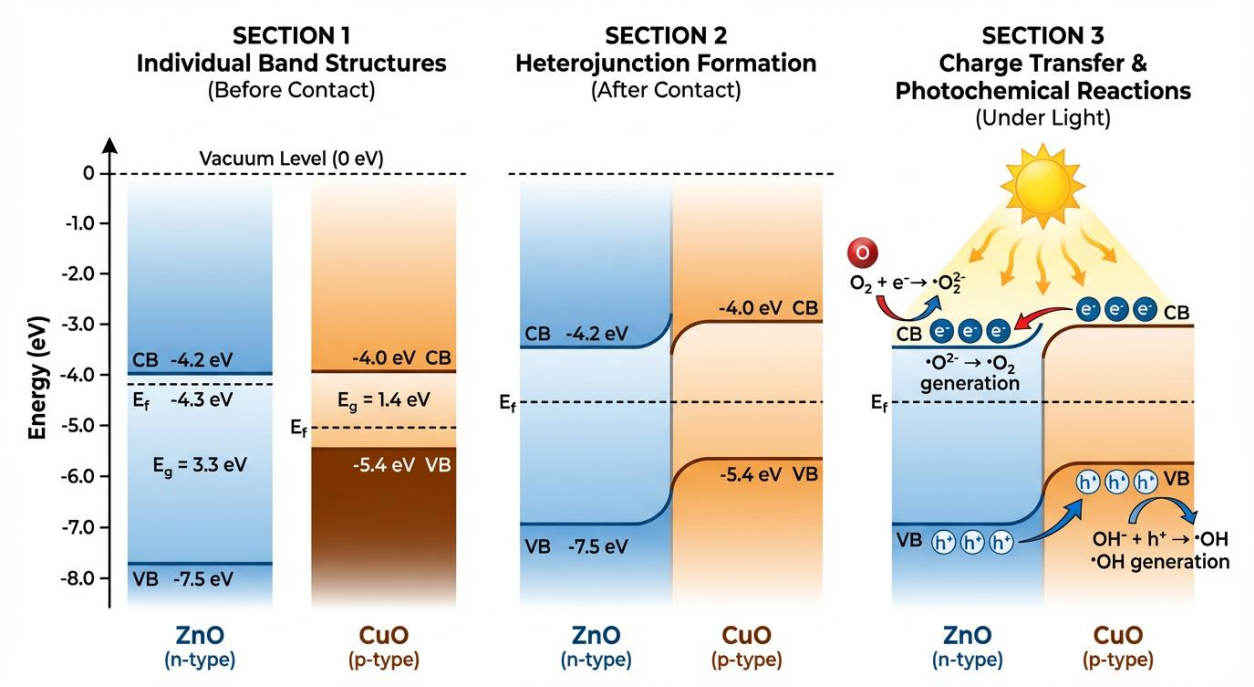

Figure III.8: Schematic representation of the band alignment and synergistic charge transfer mechanism in the ZnO/CuO heterojunction.

Furthermore, the integration of magnetic cores (Fe_3O_4) functionalized with biopolymers like chitosan [3]or decorated with plasmonic metals like silver [4]serves a dual purpose. Structurally, these matrices provide an extraordinarily high surface-area-to-volume ratio with abundant active

binding sites. Operationally, the magnetic core introduces the crucial advantage of rapid and cost-effective post-treatment recoverability using external magnetic fields. The cumulative experimental data, encompassing targeted pollutants, optimized reaction times, kinetic models, and maximum removal efficiencies across all examined nanomaterials, is comprehensively summarized and compared in **Table III.1**.

Table III.1: Summary of green-synthesized nanomaterials, targeted pollutants, and kinetic models.

Kinetic / Isotherm Model	***Optimal Time***	***Max. Removal Efficiency (%)***	***Target Pollutants***	***Plant Extract Used***	***Nanomaterial / Nanocomposite***	***Ref***
Pseudo-first-order (kinetics), Freundlich (isotherm)	30 - 20 min	100% (Cr, Mo, Sb), 99% (others), 88% (OIW), 85% (TSS)	Heavy metals (Cr, Mo, Sb, Pb), OIW, TSS	*Pistacia lentiscus*	MgO@SnO_2@PVP	[2]
4- step diffusion mechanism	24 h	Pb (84.1%), Zn (74.6%), Se (72.3%), Cr (73.7%), As (24.9%)	Heavy metals in sludge (Pb, Zn, As)	*Mentha pulegium*	Ca/α-Fe_2O_3/ZnO/CuO	[13]
Pseudo-first-order kinetics	30 min (metals), 75 min (dyes)	100% (metals), 99% (MB), 98.4% (O-TB), 90% (OIW), 78% (TSS)	Heavy metals (11 metals), Dyes (MB, O-TB), OIW, TSS	*Laurus & nobilis* Shrimp Shells	CS/Fe_3O_4 (Chitosan-coated)	[3]

Kinetic / Isotherm Model	*Optimal Time*	*Max. Removal Efficiency (%)*	*Target Pollutants*	*Plant Extract Used*	*Nanomaterial / Nanocomposite*	*Ref*
Pseudo-first-order (kinetics), half-life ($t_{1/2}$)	30 min (metals), 120 min (dyes)	100% (metals), 98% (TPH), 96.8% (RB), 93.8% (TB), 90.1% (MB), 91.8% (TSS)	Heavy metals (10 metals), TPH, Dyes (RB, TB, MB)	*Laurus nobilis*	$Ag@Fe_3O_4$	[4]
Langmuir & Freundlich (isotherms), pseudo-first-order & pseudo-second-order (kinetics)	30 min	100% (metals under optimal conditions), 100% (OIW, TSS, COD)	Heavy metals (11 metals), OIW, TSS, COD	*Mentha pulegium*	ZnO@CuO	[8]
First and Second-order kinetics	30 min	100% (metals), 80% (OIW), 70% (TSS)	Heavy metals (11 metals), OIW, TSS	*Portulaca oleracea*	α-Fe_2O_3, CuO, ZnO	[5]

III.7 Environmental Significance and Future Perspectives

Although the reviewed studies demonstrate highly promising results for the remediation of complex wastewater contaminants, several critical challenges remain before large scale industrial application can be fully achieved. Addressing these limitations is crucial for transitioning from laboratory scale success to real world environmental solutions. Primarily, transitioning the green synthesis of nanoparticles to industrial mass production while maintaining uniform size,

morphology, and high catalytic reactivity remains a significant engineering hurdle. Additionally, despite the advantages of magnetic separation observed in specific nanocomposites, designing efficient and cost-effective recovery systems for non-magnetic nanomaterials in continuous flow industrial plants requires further optimization. Furthermore, the long term ecotoxicity and secondary environmental impacts of releasing residual nanoscale metals into aquatic ecosystems are not yet fully understood and demand comprehensive lifecycle assessments. Finally, the overall economic feasibility, encompassing the continuous sourcing of plant extracts, operational energy requirements, and the integration of these advanced nanomaterials into existing wastewater treatment infrastructures, must be thoroughly evaluated. To bridge these gaps, future research should focus on developing scalable and reproducible synthesis methods, improving the long-term structural stability of nanoparticles under harsh operating conditions, and rigorously evaluating the environmental safety of nanomaterials used in water treatment technologies.


General Conclusion

General Conclusion

The escalating global water crisis, exacerbated by complex industrial and petroleum effluents, necessitates the development of advanced and sustainable remediation technologies[72]. This thesis has systematically evaluated the paradigm shift from conventional wastewater treatment to the innovative application of green synthesized metal oxide nanomaterials. By leveraging plant mediated synthesis routes, utilizing aqueous extracts from diverse botanical sources, researchers have successfully fabricated highly reactive nanoparticles and complex nanocomposites while entirely eliminating the need for toxic chemical precursors. This eco-friendly approach not only adheres to the fundamental principles of green chemistry but also imparts superior structural stability and functional surface reactivity to the synthesized materials[73]. Comprehensive analysis of the reviewed experimental data demonstrates that these biogenic nanomaterials exhibit extraordinary capabilities in sequestering highly toxic heavy metals, catalytically degrading recalcitrant organic dyes, and destabilizing complex oil in water emulsions. The strategic engineering of these materials, particularly the integration of magnetic cores and the formation of multimetallic heterojunctions, has fundamentally resolved the intrinsic limitations of bare nanoparticles. These advanced configurations ensure rapid electron hole separation for superior photocatalytic activity, maximize targeted adsorption capacities, and enable the practical recovery of the catalysts via external magnetic fields[74]. Furthermore, their demonstrated structural integrity and consistently high removal efficiencies across multiple regeneration cycles strongly underscore their economic viability for continuous industrial operations. Moving forward, while laboratory scale findings are exceptionally promising, the transition toward full scale industrial implementation requires addressing several critical engineering hurdles. Future research must prioritize the scalable mass production of these green nanomaterials, the optimization of continuous flow recovery systems, and rigorous lifecycle assessments to guarantee their long term ecotoxicological safety. Ultimately, the convergence of green chemistry and nanotechnology presents a powerful, eco-friendly, and highly effective framework for resolving the most pressing industrial wastewater challenges and advancing global environmental sustainability[75].

References

[1] A. Boretti, “Global Water Insecurity Accelerating: A Multidimensional Reassessment Integrating Scarcity, Pollution, Geopolitics, and Equity Towards 2050,” *World Water Policy,* vol. 12, no. 1, p. e70062, 2026.

[2] C. Salmi, S. E. Laouini, S. Meneceur, and H. A. Mohammed, “Biosynthesized MgO@ SnO2 nanocomposite and their modification with polyvinylpyrrolidone. Efficiency for removal of heavy metals and contaminants from industrial petroleum wastewater,” *Clean Technol. Environ. Policy,* vol. 26, no. 8, pp. 2483–2502, 2024.

[3] H. A. Mohammed *et al.*, “Efficient removal of heavy metals, dyes, and contaminants from industrial wastewater using chitosan-coated Fe3O4 nanocomposites: biosynthesis, characterizations, and performance evaluation,” *Biomass Convers. Biorefinery,* vol. 14, no. 23, pp. 30719–30734, 2024.

[4] G. G. Hasan *et al.*, “Efficient treatment of oily wastewater, antibacterial activity, and photodegradation of organic dyes using biosynthesized Ag@ Fe3O4 nanocomposite,” *Bioprocess Biosyst. Eng.*, vol. 47, no. 1, pp. 75–90, 2024.

[5] A. Bouafia *et al.*, “Removal of hydrocarbons and heavy metals from petroleum water by modern green nanotechnology methods,” *Sci. Rep.*, vol. 13, no. 1, p. 5637, 2023.

[6] C. K. Singh *et al.*, “Managing the complexity of emerging contaminants in aquatic environments: exploring their ecotoxicological impacts, detection techniques, and the use of innovative technologies for their remediation,” *Discov. Catal.*, vol. 2, no. 1, p. 9, 2025.

[7] S. Aluvihara, S. F. Alam, M. H. Omar, A. Hilonga, A. Zaryab, and S. Sadeg, “Eco-friendly and Cost-effective Water Treatment and Wastewater Treatment Technologies: A Review,” *Am. J. Water Sci. Eng.*, vol. 11, no. 3, pp. 74–85, 2025.

[8] S. Meneceur *et al.*, “Removal efficiency of heavy metals, oily in water, total suspended solids, and chemical oxygen demand from industrial petroleum wastewater by modern green nanocomposite methods,” *J. Environ. Chem. Eng.*, vol. 11, no. 6, p. 111209, 2023.

[9] P. J. Welz, “Biosand reactors for municipal and industrial wastewater treatment: status quo, challenges and opportunities,” *Processes*, vol. 12, no. 4, p. 641, 2024.

[10] B. S. Rasool, A. K. Abbas, and R. Haddad, “Photocatalytic innovations in environmental

remediation: mechanisms, materials, and challenges for persistent organic pollutant removal," *Environ. Monit. Assess.*, vol. 197, no. 10, p. 1086, 2025.

[11] M. Kiani, "Nanomaterials unveiled: catalyzing the future of technological innovation," *Available SSRN 5086632*, 2025.

[12] R. Shakeel *et al.*, "Multifunctional nanomaterials in materials chemistry: A cross-disciplinary review of applications in energy, environment, catalysis, and biomedicine," *Sch. J. Eng. Technol.*, vol. 8, pp. 673–707, 2025.

[13] A. Khezzane, A. Saoud, A. Bouafia, S. Meneceur, and F. Younsi, "Eco-friendly Ca/α-Fe2O3/ZnO/CuO nanocomposite: Green synthesis, characterization, and high-efficiency heavy metal removal from contaminated sludge," *Environ. Prog. Sustain. Energy*, p. e70207.

[14] A. Mohan, S. Rajendran, and N. Palani, "Sustainable synthesis of iron oxide nanoparticles using phytochemicals: mechanisms, functionalization strategies, applications and future perspectives," *Mater. Sci Eng*, vol. 9, no. 2, pp. 36–54, 2025.

[15] M. A. Ahmed, S. A. Mahmoud, and A. A. Mohamed, "Interfacially engineered metal oxide nanocomposites for enhanced photocatalytic degradation of pollutants and energy applications," *RSC Adv.*, vol. 15, no. 20, pp. 15561–15603, 2025.

[16] M. A. Alam, S. Pal, S. Pal, A. Dutta, and M. Mandal, "Impacts of Industrial Effluents on Plants and Their Effects on the Food Chain," in *Plant-Microbe Interaction under Xenobiotic Exposure*, Springer, 2025, pp. 197–242.

[17] H. Chang and A. R. Ross, "Climate change, urbanization, and water resources," *Portl. Springer*, vol. 198, 2024.

[18] R. K. Tamrakar, S. Butoliya, and K. Upadhyay, "Water pollution: sources, causes, and effects," in *Current Advancements in Nanomaterials for Wastewater Remediation*, Elsevier, 2026, pp. 31–50.

[19] P. K. Singh *et al.*, "Critical review on toxic contaminants in surface water ecosystem: sources, monitoring, and its impact on human health," *Environ. Sci. Pollut. Res.*, vol. 31, no. 45, pp. 56428–56462, 2024.

[20] S. Thakur, A. Chandra, V. Kumar, and S. Bharti, "Environmental pollutants: endocrine disruptors/pesticides/reactive dyes and inorganic toxic compounds metals, radionuclides,

and metalloids and their impact on the ecosystem," in *Biotechnology for environmental sustainability*, Springer, 2025, pp. 55–100.

[21] G. Singh, J. Gupta, Kartik, and A. Rana, "Water Pollution and Threats to Aquatic Biodiversity," in *Biotechnology Innovations for a Sustainable Future: Integrating Clean Energy, Life on the Planet, Clean Water, and Climate Action*, Springer, 2026, pp. 1271–1288.

[22] K. Jomova, S. Y. Alomar, E. Nepovimova, K. Kuca, and M. Valko, "Heavy metals: toxicity and human health effects," *Arch. Toxicol.*, vol. 99, no. 1, pp. 153–209, 2025.

[23] S. Liu, J. Liu, Y. Wang, F. Deng, and Z. Deng, "Oxidative stress: signaling pathways, biological functions, and disease," *MedComm*, vol. 6, no. 7, p. e70268, 2025.

[24] A. Generalova, S. Davidova, and G. Satchanska, "The mechanisms of lead toxicity in living organisms," *J. xenobiotics*, vol. 15, no. 5, p. 146, 2025.

[25] Ankush, Ritambhara, S. Lamba, Deepika, and R. Prakash, "Cadmium in environment—An overview," *Cadmium Toxic. Water Challenges Solut.*, pp. 3–20, 2024.

[26] M. Shahid, M. Danish, W. A. Ansari, S. Ali, M. A. Almalki, and M. Alfredan, "Decoding heavy metals ($Cd2^{+}$ and Cr^{6+})/metalloid ($As3^{+}$) toxicity: unmasking physiological, biochemical and genotoxic consequences in green chili," *Sci. Rep.*, 2026.

[27] T. Parangi and S. Pathan, *Materials for Dye Degradation*. CRC Press, 2025.

[28] A. Chauhan, A. Fishta, R. Thakur, and R. Banerjee, "Impact of Climate Change on Aquatic Flora and Fauna," in *Biotechnology Innovations for a Sustainable Future: Integrating Clean Energy, Life on the Planet, Clean Water, and Climate Action*, Springer, 2026, pp. 1809–1844.

[29] S. Dey, A. Das, K. Mallick, A. Sahu, and A. P. Das, "Environmental petroleum waste: pollution, toxicity, sustainable remediation," in *Impact of petroleum waste on environmental pollution and its sustainable management through circular economy*, Springer, 2024, pp. 159–175.

[30] A. Malik, "Separation of Diluted Oil Emulsions for Water Purification: A Comprehensive Review of Techniques, Materials, and Future Trends," in *Publisher. agency: Proceedings of the 10th International Scientific Conference «Scientific Results»(June 5-6, 2025). Rome, Italy, 2025. 449p*, University of Bari Aldo Moro, 2025, p. 318.

[31] A. R. M. Salah, “Aromatic Compounds: Structural Principles, Reactivity Models, and Industrial Applications,” 2025.

[32] H. M. Wolgien-Lowe, “From Fermenter to Farm: Downstream Processing of Single Cell Protein,” 2025.

[33] D. Sah, “Potential of Bioremediation and Biosurfactant Production by Native Bacterial Consortium Isolated from Petroleum Contaminated Soil,” 2023.

[34] O. T. Ogunwumi, A. F. Adeniyi, M. C. Angus, and O. S. Oche, “Biological wastewater treatment,” *Wastewater Treat. Sludge Manag. Syst. Gutter-to-Good Approaches Gutter-to-Good Approaches*, p. 221, 2025.

[35] A. Kumar, R. Kumar, A. Parnian, M. Mahbod, and M. A. E. AbdelRahman, “Bioremediation: a better technique for wastewater treatment and resource recovery,” in *Biotechnologies for Wastewater Treatment and Resource Recovery*, Elsevier, 2025, pp. 17–32.

[36] K. Kannathasan *et al.*, “A scalable and chemical-free strategy for antifouling ultrafiltration PVDF membranes via hydrophilic macromolecular surface modification,” *J. Mater. Sci.*, vol. 60, no. 44, pp. 21900–21924, 2025.

[37] S. Hussain *et al.*, “From atomic nuclei to nanostructures: Harnessing the convergence of nuclear physics, particle dynamics, and nanotechnology to transform energy, revolutionize medicine, and advance environmental sustainability,” *Glob. Sci. Acad. Res. J. Multidiscip. Stud*, vol. 4, pp. 87–117, 2025.

[38] M. Rahman *et al.*, “Nanotechnology and thermodynamics: a comprehensive review,” *Nanomater. Energy*, vol. 14, no. 2, pp. 109–134, 2025.

[39] W. Guo *et al.*, “Tailoring Materials Design for Aqueous Energy Storage and Conversion through Electrochemical Reconstruction,” *Chem. Rev.*, 2026.

[40] B. D. Cardoso *et al.*, “Progress in nanofluid technology: From conventional to green nanofluids for biomedical, heat transfer, and machining applications,” *Nanomaterials*, vol. 15, no. 16, p. 1242, 2025.

[41] A. Sati, T. N. Ranade, S. N. Mali, H. K. Ahmad Yasin, and A. Pratap, “Silver nanoparticles (AgNPs): comprehensive insights into bio/synthesis, key influencing factors, multifaceted applications, and toxicity─ a 2024 update,” *ACS omega*, vol. 10, no. 8, pp.

7549–7582, 2025.

[42] S. S. Chowdhury, N. Ibnat, M. Hasan, and A. Ghosh, “Medicinal Plant-Based nanoparticle synthesis and their diverse applications,” in *Ethnopharmacology and OMICS advances in medicinal plants volume 2: revealing the secrets of medicinal plants*, Springer, 2024, pp. 213–250.

[43] S. Zhang *et al.*, “Green synthesis, biomedical effects, and future trends of Ag/ZnO bimetallic nanoparticles: An update,” *Nanotechnol. Rev.*, vol. 14, no. 1, p. 20250186, 2025.

[44] A. ur R. Khan, M. Z. Khan, A. Ahmad, J. Li, and L. Song, “Unlocking the biomedical potential of epigallocatechin-3-gallate: A review on bioactive properties, stability limitations, and nano-delivery innovations,” *Nat. Prod. Res.*, pp. 1–23, 2025.

[45] G. Shuangmei, Y. Changying, L. Min, and L. Xiaobo, “Study on the correlation between proton transfer of phenolic hydroxyl groups of 6 flavonoid compounds and their antioxidant activities,” *Biochim. Biophys. Acta (BBA)-Biomembranes*, p. 184444, 2025.

[46] R. Baby, M. Z. Hussein, A. H. Abdullah, and Z. Zainal, “Nanomaterials for the treatment of heavy metal contaminated water,” *Polymers (Basel).*, vol. 14, no. 3, p. 583, 2022.

[47] F. L. García-Larez *et al.*, “Polysaccharides from agro-industrial waste and by-products: an overview on green synthesis of metallic nanoparticles—an ecofriendly approach,” *Polysaccharides*, vol. 6, no. 2, p. 53, 2025.

[48] M. G. W. Gangurde and B. A. Shingade, *Advances in Nanoscience and Nanotechnology*. Addition Publishing House, 2025.

[49] H. Rafeeq, A. Hussain, A. Ambreen, M. Waqas, M. Bilal, and H. M. N. Iqbal, “Functionalized nanoparticles and their environmental remediation potential: a review,” *J. Nanostructure Chem.*, vol. 12, no. 6, pp. 1007–1031, 2022.

[50] S. Gulati, S. K. Pandey, Tamanna, R. Jeena, and S. Jha, “Next-generation environmental guardians: advanced nanosensors for precision remediation and sustainable monitoring,” *Water, Air, Soil Pollut.*, vol. 236, no. 12, p. 804, 2025.

[51] S. TL, K. J. Rao, and T. Korumilli, “Natural biogenic templates for nanomaterial synthesis: advances, applications, and environmental perspectives,” *ACS Biomater. Sci. Eng.*, vol. 11, no. 3, pp. 1291–1316, 2025.

[52] V. Losetty *et al.*, “Transformative applications of polymer-based metal oxide nanocomposites in medicine, industry, and environmental remediation: a review,” *J. Inorg. Organomet. Polym. Mater.*, vol. 36, no. 1, pp. 64–96, 2026.

[53] J. Tripathy *et al.*, “Advances in nanoparticles and nanocomposites for water and wastewater treatment: a review,” *Water*, vol. 16, no. 11, p. 1481, 2024.

[54] I.-C. Radu, A.-M. Vadureanu, D.-E. Cozorici, E. Blanzeanu, and C. Zaharia, “Advancing sustainability in modern polymer processing: strategies for waste resource recovery and circular economy integration,” *Polymers (Basel).*, vol. 17, no. 4, p. 522, 2025.

[55] K. Alam, “Development and production of Bimetallic Nanomaterials by means of a Spinning disc reactor for environmental and industrial applications,” 2025.

[56] Y. Yao *et al.*, “Roadmap for next-generation electrochemical energy storage technologies: secondary batteries and supercapacitors,” *ACS Nano*, vol. 19, no. 34, pp. 30568–30687, 2025.

[57] B. Biswas, S. Asif, R. Puria, and A. Thakur, “A novel and robust method for investigating fungal biofilm,” *Bio-protocol*, vol. 15, no. 1, 2025.

[58] K. G. Steinhäuser and M. Große Ophoff, “The need for change: a roadmap for the sustainable transformation of the chemical industry,” *Sustain. Chem.*, vol. 6, no. 2, p. 16, 2025.

[59] S. Basu and N. M. Nadella, “Water Management in Upstream and Midstream Operations,” in *Water Management in Petroleum Industries*, Springer, 2025, pp. 131–184.

[60] R. K. Paul and M. Ahmaruzzaman, “Advanced photocatalytic degradation of POPs and other contaminants: a comprehensive review on nanocomposites and heterojunctions,” *RSC Adv.*, vol. 15, no. 38, pp. 31313–31359, 2025.

[61] M. A. Rahaman *et al.*, “Crystallographic phase bibliography and quantitative phase analysis of TiO2 nanocrystals: A rietveld refinement insight,” *Next Res.*, vol. 2, no. 3, p. 100469, 2025.

[62] C. M. Rafeeq, R. Karim, and P. P. Manzur Ali, “Nanoscale materials and their properties,” in *Plant nanotechnology fundamentals and methodologies*, Springer, 2025, pp. 39–71.

[63] J. Wang, X. Liu, W. Li, Y. Tu, H. Deng, and J. Du, “Deciphering heavy metal adsorption capacity of soil based on its physicochemical properties and adsorption reaction time using

machine learning," *J. Environ. Chem. Eng.*, vol. 13, no. 3, p. 116913, 2025.

[64] D. Wu *et al.*, "The role of adsorption and diffusion in improving the selectivity and reactivity of zeolite catalysts," *Chem. Soc. Rev.*, vol. 54, no. 20, pp. 9192–9244, 2025.

[65] V. Girotra, P. Kaushik, and D. Vaya, "Exploring sustainable synthesis paths: a comprehensive review of environmentally friendly methods for fabricating nanomaterials through green chemistry approaches," *Turkish J. Chem.*, vol. 48, no. 5, pp. 703–725, 2024.

[66] S. Pasieczna-Patkowska, M. Cichy, and J. Flieger, "Application of Fourier transform infrared (FTIR) spectroscopy in characterization of green synthesized nanoparticles," *Molecules*, vol. 30, no. 3, p. 684, 2025.

[67] G. W. Bayisa, "Biogenic Synthesis of Silver Nanostructures from Propolis and Bee Pollen: Antibacterial, Antioxidant, and Biosensing Applications," 2025.

[68] W. A. A. Mohamed *et al.*, "Principles, applications and future prospects in photodegradation systems," *Nanotechnol. Rev.*, vol. 14, no. 1, p. 20250159, 2025.

[69] A. Haleem *et al.*, "In-depth photocatalytic degradation mechanism of the extensively used dyes malachite green, methylene blue, Congo red, and rhodamine B via covalent organic framework-based photocatalysts," *Water*, vol. 16, no. 11, p. 1588, 2024.

[70] M. Zhang *et al.*, "A near-infrared light responsive nanoheterojunction for antibacterial and anti-inflammatory applications through programmed ROS regulation," *J. Colloid Interface Sci.*, p. 138489, 2025.

[71] P. Mani *et al.*, "Scaling up of photocatalytic systems for large-scale hydrogen generation," *Appl. Phys. Rev.*, vol. 12, no. 1, 2025.

[72] F. A. S. Islam, "Advanced wastewater treatment technologies in addressing future water scarcity through resource recovery and reuse," *J. Eng. Res. Reports*, vol. 27, no. 5, pp. 370–398, 2025.

[73] T. Sajini and J. Joseph, "Microwave-assisted synthesis of nanomaterials: a green chemistry perspective and sustainability assessment," *RSC Sustain.*, vol. 3, no. 11, pp. 4911–4935, 2025.

[74] R. Li *et al.*, "Research advances in magnetic field-assisted photocatalysis," *Adv. Funct. Mater.*, vol. 34, no. 33, p. 2316725, 2024.

[75] M. A. Abdel-Fatah and E. F. Ewies, "Green nanotechnology for sustainable ecosystems:

innovations in pollution remediation and resource recovery," *Egypt. J. Chem.*, vol. 68, no. 10, pp. 621–633, 2025.

ABSTRACT

This thesis explores the theoretical analysis and literature review concerning the green synthesis, characterization, and environmental applications of metal oxide-based nanocomposites for the effective removal of complex pollutants from aqueous media. The work is framed within the context of sustainable nanotechnology and focuses on multifunctional nanocomposite systems combining metal oxide nanoparticles with biopolymers or magnetic structures to enhance photocatalytic and adsorptive performance.

Several innovative nanocomposite systems were comprehensively analyzed and evaluated:

1. • **MgO@SnO_2/PVP** nanocomposites for the adsorption of heavy metals, oil-in-water (OIW) emulsions, and total suspended solids (TSS) from industrial petroleum wastewater.
2. • **Ca/α-Fe_2O_3/ZnO/CuO** quaternary nanocomposites for high-efficiency heavy metal removal from contaminated sludge.
3. • **CS/Fe_3O_4** (chitosan-coated) and **Ag@Fe_3O_4** nanocomposites for the simultaneous removal of heavy metals and rapid photodegradation of organic dyes (Methylene Blue and Rose Bengal).
4. • **ZnO@CuO** heterojunctions and single metal oxides (**α-Fe_2O_3, CuO, ZnO**) for the degradation of total petroleum hydrocarbons (TPH) and advanced purification of real petroleum effluents.

All nanomaterials were synthesized using eco-friendly routes, employing natural plant extracts (*Mentha pulegium*, *Laurus nobilis*, *Pistacia lentiscus*, and *Portulaca oleracea*) as reducing and capping agents. Structural, morphological, optical, and surface properties were characterized using XRD, FTIR, SEM, EDX, UV–Vis spectroscopy, and zeta potential analysis. The performance of the nanocomposites was evaluated through adsorption and photodegradation experimental data. Kinetic (pseudo-first and pseudo-second-order) and isotherm (Langmuir and Freundlich) models were applied to describe the adsorption mechanisms.

Keywords: Green synthesis, Metal oxide nanoparticles, Petroleum wastewater, Heavy metals adsorption, Photocatalytic degradation, Sustainable nanotechnology.